

Distance Metric Learning for Graph Structured Data

Tomoki Yoshida¹, Ichiro Takeuchi^{1,2,3}, and Masayuki Karasuyama^{1,2,4}

¹Nagoya Institute of Technology

²National Institute for Material Science

³RIKEN Center for Advanced Intelligence Project

⁴Japan Science and Technology Agency

yoshida.t.mllab.nit@gmail.com, {takeuchi.ichiro,karasuyama}@nitech.ac.jp

Abstract

Graphs are versatile tools for representing structured data. As a result, a variety of machine learning methods have been studied for graph data analysis. Although many such learning methods depend on the measurement of differences between input graphs, defining an appropriate distance metric for graphs remains a controversial issue. Hence, we propose a supervised distance metric learning method for the graph classification problem. Our method, named *interpretable graph metric learning* (IGML), learns discriminative metrics in a subgraph-based feature space, which has a strong graph representation capability. By introducing a sparsity-inducing penalty on the weight of each subgraph, IGML can identify a small number of important subgraphs that can provide insight into the given classification task. Because our formulation has a large number of optimization variables, an efficient algorithm that uses pruning techniques based on *safe screening* and *working set selection* methods is also proposed. An important property of IGML is that solution optimality is guaranteed because the problem is formulated as a convex problem and our pruning strategies only discard unnecessary subgraphs. Furthermore, we show that IGML is also applicable to other structured data such as itemset and sequence data, and that it can incorporate vertex-label similarity by using a transportation-based subgraph feature. We empirically evaluate the computational efficiency and classification performance of IGML on several benchmark datasets and provide some illustrative examples of how IGML identifies important subgraphs from a given graph dataset.

1 Introduction

Because of the growing diversity of data science applications, machine learning methods must adapt to a variety of complicated structured data, from which it is often difficult to obtain typical numerical vector representations of input objects. A standard approach to modeling structured data is to employ *graphs*. For example, graph-based representations are prevalent in domains such as chemo- and bio- informatics. In this study, we particularly focus on the case in which a data instance is represented as a pair of a graph and its associated class label.

Although numerous machine learning methods explicitly or implicitly depend on how to measure differences between input objects, defining an appropriate distance metric on graphs remains a controversial issue in the field. A widely accepted approach is the *graph kernel* (Gärtner et al., 2003; Vishwanathan et al., 2010), which enables to apply machine learning methods to graph data without requiring explicit vector representations. Another popular approach would be to use neural networks (Atwood and Towsley, 2016; Narayanan et al., 2017), from which a suitable representation can be learned while avoiding to explicitly define a metric. However, in these approaches, it is difficult to create a metric that explicitly extracts significant sub-structures, i.e., subgraphs. Identifying discriminative subgraphs in an interpretable manner can be insightful for many graph classification tasks. In particular, graph representation is prevalent in

scientific data analysis. For example, chemical compounds are often represented by graphs; thus, finding subgraphs that have a strong effect on a target label (e.g., toxicity) is informative. Other examples of graph representations are protein 3D structures and crystalline substances (e.g., Brinda and Vishveshwara, 2005; Xie and Grossman, 2018), where the automatic identification of important sub-structures is expected to provide an insight behind correlation between structures and target labels. Further details of the previous studies are discussed in Section 2.

We propose a supervised method that obtains a metric for graphs, thereby achieving both high predictive performance and interpretability. Our method, named *interpretable graph metric learning* (IGML), combines the concept of *metric learning* (e.g., Weinberger and Saul, 2009; Davis et al., 2007) with a subgraph representation, where each graph is represented by a set of its subgraphs. IGML optimizes a metric that assigns a weight $m_{i(H)} \geq 0$ to each subgraph H contained in a given graph G . Let $\phi_H(G)$ be a feature of the graph G that is monotonically non-decreasing with respect to the frequency of subgraph H of G . Note that we assume that subgraphs are counted without overlapped vertices and edges throughout the study. We consider the following squared distance between two graphs G and G' :

$$d_{\mathbf{m}}(G, G') := \sum_{H \in \mathcal{G}} m_{i(H)} (\phi_H(G) - \phi_H(G'))^2, \quad (1)$$

where \mathcal{G} is the set of all connected graphs. Although it is known that the subgraph approach has strong graph representation capability (e.g. Gärtner et al., 2003), naïve calculation is obviously infeasible unless the weight parameters have some special structure.

We formulate IGML as a supervised learning problem of the distance function (1) using a pairwise loss function of metric learning (Davis et al., 2007) with a sparse penalty on $m_{i(H)}$. The resulting optimization problem is computationally infeasible at a glance, because the number of weight parameters is equal to the number of possible subgraphs, which is usually intractable. We overcome this difficulty by introducing *safe screening* (Ghaoui et al., 2010) and *working set selection* (Fan et al., 2008) approaches. Both of these approaches can significantly reduce the number of variables, and further, they can be combined with a *pruning* strategy on the tree traverse of *graph mining*. These optimization tricks are inspired by two recent studies (Nakagawa et al., 2016) and (Morvan and Vert, 2018), which developed safe screening- and working set- based pruning for a linear prediction model with the LASSO penalty, respectively. By combining these two techniques, we constructed a path-wise optimization method that can obtain a sparse solution of the weight parameter $m_{i(H)}$ without directly enumerating all possible subgraphs.

To the best of our knowledge, no previous studies can provide an interpretable subgraph-based metric learned in a supervised manner. The advantages of IGML can be summarized as follows:

- Because IGML is formulated as a convex optimization problem, the global optimal can be found by the standard gradient-based optimization.
- The safe screening- and working set-based optimization algorithms make our problem practically tractable without sacrificing optimality.
- We can identify a small number of important subgraphs that discriminate different classes. This implies that the resulting metric is easy to compute and highly interpretable, making it useful for a variety of subsequent data analyses. For example, applying the nearest neighbor classification or decision tree on the learned space would be effective.

Moreover, we propose three extensions of IGML. First, we show that IGML is directly applicable to other structured data, such as itemset and sequence data. Second, its application to a triplet based loss function is discussed. Third, we extend IGML to allow similarity information of vertex-labels to be incorporated. We empirically verify the superior or comparable prediction performance of IGML to other existing graph classification methods (most of which are not interpretable). We also show some examples of extracted subgraphs and data analyses on the learned metric space.

The remainder of this paper is organized as follows. In Section 2, we review previous studies on graph data analysis. In Section 3, we introduce a formulation of our proposed IGML. Section 4 discusses strategies to reduce the size of the IGML optimization problem. The detailed computational procedure of IGML is described in Section 5. Three extensions of IGML are presented in Section 6. Section 7 reports our empirical evaluation of the effectiveness of IGML on several benchmark datasets.

Note that this paper is an extended version of a preliminary conference paper (Yoshida et al., 2019a). The source code of the program used in our experiments is available at <https://github.com/takeuchi-lab/Learning-Interpretable-Metric-between-Graphs>.

2 Related Work

Kernel-based approaches have been widely studied for graph data analysis, and they can provide a metric of graph data in a reproducing kernel Hilbert space. In particular, subgraph-based graph kernels are closely related to our study. The graphlet kernel (Shervashidze et al., 2009) creates a kernel through small subgraphs with only about 3–5 vertices, which are called graphlets. The neighborhood subgraph pairwise distance kernel (Costa and Grave, 2010) selects pairs of subgraphs from a graph and counts the number of pairs identical to those in another graph. The subgraph matching kernel (Kriege and Mutzel, 2012) identifies common subgraphs based on cliques in the product graph of two graphs. The feature space created by these subgraph-based kernels is easy to interpret. However, because the above approaches are unsupervised, it is fundamentally impossible to eliminate subgraphs that are unnecessary for a specific target classification task. Therefore, for example, to create the entire kernel matrix of training data, all the candidate subgraphs in the data must be enumerated once, which becomes intractable even for small-sized subgraphs. In contrast, we consider dynamically “pruning” unnecessary subgraphs through a supervised formulation of metric learning. As we will demonstrate in our later experimental results, this significantly reduces the enumeration cost, allowing our proposed algorithm to deal with the larger size of subgraphs than the simple subgraph based kernels.

There are many other kernels including the shortest path (Borgwardt and Kriegel, 2005)-, random walk (Vishwanathan et al., 2010; Sugiyama and Borgwardt, 2015; Zhang et al., 2018b)-, and spectrum-based (Kondor and Borgwardt, 2008; Kondor et al., 2009; Kondor and Pan, 2016; Verma and Zhang, 2017) approaches. The Weisfeiler–Lehman (WL) kernel (Shervashidze and Borgwardt, 2009; Shervashidze et al., 2011), which is based on the graph isomorphism test, is a popular and empirically successful kernel that has been employed in many studies (Yanardag and Vishwanathan, 2015; Niepert et al., 2016; Narayanan et al., 2017; Zhang et al., 2018a). Again, all such approaches are unsupervised, and it is difficult to interpret results from the perspective of sub-structures of a graph. Although several kernels deal with continuous attributes on vertices (Feragen et al., 2013; Orsini et al., 2015; Su et al., 2016; Morris et al., 2016), we only focus on the cases where vertex-labels are discrete due to the associated interpretability.

Because obtaining a good metric is an essential task in data analysis, metric learning has been extensively studied to date, as reviewed in (Li and Tian, 2018). However, due to its computational difficulty, metric learning for graph data has not been widely studied. A few studies have considered the *edit distance* approaches. For example, Bellet et al. (2012) presented a method for learning a similarity function through an edit distance in a supervised manner. Another approach probabilistically formulates the editing process of the graph and estimates the parameters using labeled data Neuhaus and Bunke (2007). However, these approaches cannot provide any clear interpretation of the resulting metric in term of the subgraphs.

Likewise, the deep neural network (DNN) is a standard approach to graph data analysis. The deep graph kernel (Yanardag and Vishwanathan, 2015) incorporates neural language modeling, where decomposed sub-structures of a graph are regarded as sentences. The PATCHY-SAN (Niepert et al., 2016) and DGCNN (Zhang et al., 2018a) convert a graph to a tensor by using the WL-Kernel and convolute it. Several other studies also have combined popular convolution techniques with graph data (Tixier et al., 2018; Atwood and Towsley, 2016; Simonovsky and Komodakis, 2017). These approaches are supervised, but the interpretability of these DNNs is obviously relatively low. *Attention* enhances the interpretability of deep learning, but extracting important subgraphs is difficult because attention algorithms for graphs (Lee et al., 2018) only provides the significance of vertex transition on a graph. Another related DNN approach is representation learning. For example, sub2vec (Adhikari et al., 2018) and graph2vec (Narayanan et al., 2017) can embed graph data into a continuous space, but they are unsupervised, and it is difficult to extract substructures that characterize different classes. There are other fingerprint learning methods for graphs by neural networks (e.g. Duvenaud et al., 2015) where the contribution from each node can be evaluated for each dimension of the fingerprint. Although it is possible to highlight sub-structures for the given input graph, this does not produce important common subgraphs for prediction.

Supervised pattern mining (Cheng et al., 2008; Novak et al., 2009; Thoma et al., 2010) can be used for identifying important subgraphs by enumerating patterns with some discriminative score. However, these approaches usually 1) employ a greedy strategy to add a pattern for which global optimality cannot be guaranteed, and 2) do not optimize a metric or representation. A few other studies (Saigo et al., 2009; Nakagawa et al., 2016) have considered optimizing a linear model on the subgraph features with the LASSO penalty using graph mining. A common idea of these two methods is to traverse a graph mining tree with pruning strategies derived from optimality conditions. Saigo et al. (2009) employed a boosting-based approach, which adds a subgraph that violates the optimality condition most severely at every iteration. It was shown that the maximum violation condition can be efficiently identified by pruning the tree without losing the final solution optimality. Nakagawa et al. (2016) derived a pruning criterion by extending *safe screening* (Ghaoui et al., 2010), which can safely eliminate unnecessary features before solving the optimization problem. This approach can also avoid enumerating the entire tree while guaranteeing the optimality, and its efficiency compared with the boosting-based approach was demonstrated empirically, mainly because it requires much fewer tree traversals. Further, Morvan and Vert (2018) proposed a similar pruning extension of *working set selection* for optimizing a higher-order interaction model. Although this paper was not for the graph data, the technique is applicable to the same subgraph-based linear model as in (Saigo et al., 2009) and (Nakagawa et al., 2016). Working set selection is a heuristic feature subset selection strategy that has been widely used in machine learning algorithms, such as support vector machines (e.g., Hsu and Lin, 2002). Unlike safe screening, this heuristic selection may eliminate necessary features in the middle of the optimization, but the optimality of the final solution can be guaranteed by iterating subset selection repeatedly until the solution converges. However, these methods can only optimize a linear prediction model. In this study, we focus on *metric learning* of graphs. Therefore, unlike the above mentioned pruning based learning methods, our aim is to learn a “distance function”. In metric learning, a distance function is typically learned from a loss function defined over a relative relation between samples (usually, pairs or triplets), by which a discriminative feature space that is generally effective for subsequent tasks, such as classification and similarity-based retrieval, is obtained. Inspired by (Nakagawa et al., 2016) and (Morvan and Vert, 2018), we derive screening and pruning rules for this setting, and further, we combine them to develop an efficient algorithm.

3 Formulation of Interpretable Graph Metric Learning

3.1 Optimization problem

Suppose that the training dataset $\{(G_i, y_i)\}_{i \in [n]}$ consists of n pairs of a graph G_i and a class label y_i , where $[n] := \{1, \dots, n\}$. Let \mathcal{G} be the set of all connected subgraphs of $\{G_i\}_{i \in [n]}$. In each graph, vertices and edges can be labeled. If $H \in \mathcal{G}$ is a connected subgraph of $G \in \mathcal{G}$, we write $H \sqsubseteq G$. Further, let $\#(H \sqsubseteq G)$ be the frequency of the subgraph H in G . Note that we adopt a definition of frequency that does not allow any vertices or edges among the counted subgraphs to overlap. As a representation of a graph G , we consider the following subgraph-based feature representation:

$$\phi_H(G) = g(\#(H \sqsubseteq G)), \text{ for } H \in \mathcal{G}, \tag{2}$$

where g is some monotonically non-decreasing and non-negative function, such as the identity function $g(x) = x$ or indicator function $g(x) = 1_{x>0}$, which takes the value 1 if $x > 0$, and 0 otherwise. It is widely known that subgraph-based features can effectively represent graphs. For example, $g(x) = x$ allows all non-isomorphic graphs to be distinguished. A similar idea was shown in (Gärtner et al., 2003) for a frequency that allows overlaps. However, this feature space is practically infeasible because the possible number of subgraphs is prohibitively large.

We focus on how to measure the distance between two graphs, which is essential for a variety of machine learning problems. We consider the following weighted squared distance between two graphs:

$$d_m(G, G') := \sum_{H \in \mathcal{G}} m_{i(H)} (\phi_H(G) - \phi_H(G'))^2,$$

where $i(H)$ is the index of the subgraph H for a weight parameter $m_{i(H)} \geq 0$. To obtain an effective and

computable distance metric, we adaptively estimate $m_{i(H)}$ such that only a small number of important subgraphs have non-zero $m_{i(H)}$ values.

Let $\mathbf{x}_i \in \mathbb{R}^p$ be the feature vector defined by concatenating $\phi_H(G_i)$ for all $H \in \mathcal{G}$ included in the training dataset. Then, we have

$$d_{\mathbf{m}}(\mathbf{x}_i, \mathbf{x}_j) = (\mathbf{x}_i - \mathbf{x}_j)^\top \text{diag}(\mathbf{m})(\mathbf{x}_i - \mathbf{x}_j) = \mathbf{m}^\top \mathbf{c}_{ij},$$

where $\mathbf{m} \in \mathbb{R}_+^p$ is a vector of $m_{i(H)}$, and $\mathbf{c}_{ij} \in \mathbb{R}^p$ is defined as $\mathbf{c}_{ij} := (\mathbf{x}_i - \mathbf{x}_j) \circ (\mathbf{x}_i - \mathbf{x}_j)$ with the element-wise product \circ .

Let $\mathcal{S}_i \subseteq [n]$ and $\mathcal{D}_i \subseteq [n]$ be the subsets of indices that are in the same and different classes to \mathbf{x}_i , respectively. For each of these sets, we select the K most similar inputs to \mathbf{x}_i by using some default metric, such as the graph kernel (further details are presented in Section 3.2). As a loss function for \mathbf{x}_i , we consider

$$\ell_i(\mathbf{m}; L, U) := \sum_{l \in \mathcal{D}_i} \ell_L(\mathbf{m}^\top \mathbf{c}_{il}) + \sum_{j \in \mathcal{S}_i} \ell_{-U}(-\mathbf{m}^\top \mathbf{c}_{ij}), \quad (3)$$

where $L, U \in \mathbb{R}_+$ are constant parameters satisfying $U \leq L$, and $\ell_t(x) = [t - x]_+^2$ is the standard squared hinge loss function with threshold $t \in \mathbb{R}$. This loss function is a variant of the pairwise loss functions used in metric learning (Davis et al., 2007). The first term in the loss function yields a penalty if \mathbf{x}_i and \mathbf{x}_l are closer than L for $l \in \mathcal{D}_i$, and the second term yields a penalty if \mathbf{x}_i and \mathbf{x}_j are more distant than U for $j \in \mathcal{S}_i$.

Let $R(\mathbf{m}) = \|\mathbf{m}\|_1 + \frac{\eta}{2} \|\mathbf{m}\|_2^2 = \mathbf{m}^\top \mathbf{1} + \frac{\eta}{2} \|\mathbf{m}\|_2^2$ be an elastic-net type sparsity-inducing penalty, where $\eta \geq 0$ is a non-negative parameter. We define our proposed IGML (*interpretable graph metric learning*) as the following regularized loss minimization problem:

$$\min_{\mathbf{m} \geq \mathbf{0}} P_\lambda(\mathbf{m}) := \sum_{i \in [n]} \ell_i(\mathbf{m}; L, U) + \lambda R(\mathbf{m}), \quad (4)$$

where $\lambda > 0$ is the regularization parameter. The solution of this problem can provide not only a discriminative metric but also insight into important subgraphs because the sparse penalty is expected to select only a small number of non-zero parameters.

Let $\boldsymbol{\alpha} \in \mathbb{R}_+^{2nK}$ be the vector of dual variables where α_{il} and α_{ij} for $i \in [n], l \in \mathcal{D}_i$, and $j \in \mathcal{S}_i$ are concatenated. The dual problem of (4) is written as follows (see Appendix A for derivation):

$$\max_{\boldsymbol{\alpha} \geq \mathbf{0}} D_\lambda(\boldsymbol{\alpha}) := -\frac{1}{4} \|\boldsymbol{\alpha}\|_2^2 + \mathbf{t}^\top \boldsymbol{\alpha} - \frac{\lambda \eta}{2} \|\mathbf{m}_\lambda(\boldsymbol{\alpha})\|_2^2, \quad (5)$$

where

$$\mathbf{m}_\lambda(\boldsymbol{\alpha}) := \frac{1}{\lambda \eta} [\mathbf{C}\boldsymbol{\alpha} - \lambda \mathbf{1}]_+, \quad (6)$$

$\mathbf{t} := [L, \dots, L, -U, \dots, -U]^\top \in \mathbb{R}^{2nK}$ and $\mathbf{C} := [\dots, \mathbf{c}_{il}, \dots, -\mathbf{c}_{ij}, \dots] \in \mathbb{R}^{p \times 2nK}$. Then, from the optimality condition, we obtain the following relationship between the primal and dual variables:

$$\alpha_{il} = -\ell'_L(\mathbf{m}^\top \mathbf{c}_{il}), \quad \alpha_{ij} = -\ell'_{-U}(-\mathbf{m}^\top \mathbf{c}_{ij}), \quad (7)$$

where $\ell'_t(x) = -2[t - x]_+$ is the derivative of ℓ_t . When the regularization parameter λ is larger than certain λ_{\max} , the optimal solution is $\mathbf{m} = \mathbf{0}$. Then, the optimal dual variables are $\alpha_{il} = -\ell'_L(0) = 2L$ and $\alpha_{ij} = -\ell'_{-U}(0) = 0$. By substituting these equations into (6), we obtain λ_{\max} as

$$\lambda_{\max} = \max_k \mathbf{C}_{k,:} \boldsymbol{\alpha}. \quad (8)$$

3.2 Selection of \mathcal{S}_i and \mathcal{D}_i

For $K = |\mathcal{S}_i| = |\mathcal{D}_i|$, in the experiments reported later, we employed the small number $K = 10$ and used a graph kernel to select samples in \mathcal{S}_i and \mathcal{D}_i . Although we simply used a pre-determined kernel, selecting the kernel (or its parameter) through cross-validation beforehand is also possible. Using only a small number

of neighbors is a common setting in metric learning. For example, Davis et al. (2007), which is a seminal work on the pairwise approach, only used $20c^2$ pairs in total, where c is the number of classes. A small K setting has two aims. First, particularly \mathcal{S}_i , adding pairs that are too far apart can be avoided under this setting. Even for a pair of samples with the same labels, enforcing such distant pairs to be close may cause over-fitting (e.g., when the sample is an outlier). Second, a small K reduces the computational cost. Because the number of pairs is $O(n^2)$, adding all of them into the loss term requires a large computational cost. In fact, these two issues are not only for the pairwise formulation but also for other relative loss functions such as the standard triplet loss, for which there exist $O(n^3)$ triplets. One potential difficulty in selecting \mathcal{D}_i and \mathcal{S}_i is the discrepancy between the initial and the optimal metric. The loss function is defined through \mathcal{D}_i and \mathcal{S}_i , which are selected based on the neighbors in the initial metric, but the optimization of the metric may change the nearest neighbors of each sample. A possible remedy for this problem is to adaptively change \mathcal{D}_i and \mathcal{S}_i in accordance with the updated metric (Takeuchi and Sugiyama, 2011), though the resulting optimality of this approach is still not known. To the best of our knowledge, this is still an open problem in metric learning, which we consider beyond the scope of this paper. In the experiments (Section 7), we show that a nearest-neighbor classifier in the learned metric with this heuristics selection of \mathcal{D}_i and \mathcal{S}_i shows better or comparable performance to standard graph classification methods, such as a graph neural network.

4 Creating a Tractable Sub-problem

Because the problems of (4) and (5) are convex, the local solution is equivalent to the global optimal. However, naïvely solving these problems is computationally intractable because of the high dimensionality of \mathbf{m} . In this section, we introduce several useful rules for restricting candidate subgraphs while maintaining the optimality of the final solution. Note that the proofs for all the lemmas and theorems are provided in the appendix.

To make the optimization problem tractable, we work with only a small subset of features during the optimization process. Let $\mathcal{F} \subseteq [p]$ be a subset of features. By fixing $m_i = 0$ for $i \notin \mathcal{F}$, we define sub-problems of the original primal P_λ and dual D_λ problems as follows:

$$\min_{\mathbf{m}_{\mathcal{F}} \geq \mathbf{0}} P_\lambda^{\mathcal{F}}(\mathbf{m}_{\mathcal{F}}) := \sum_{i \in [n]} \left[\sum_{l \in \mathcal{D}_i} \ell_L(\mathbf{m}_{\mathcal{F}}^\top \mathbf{c}_{il_{\mathcal{F}}}) + \sum_{j \in \mathcal{S}_i} \ell_{-U}(-\mathbf{m}_{\mathcal{F}}^\top \mathbf{c}_{ij_{\mathcal{F}}}) \right] + \lambda R(\mathbf{m}_{\mathcal{F}}), \quad (9)$$

$$\max_{\boldsymbol{\alpha} \geq \mathbf{0}} D_\lambda^{\mathcal{F}}(\boldsymbol{\alpha}) := -\frac{1}{4} \|\boldsymbol{\alpha}\|_2^2 + \mathbf{t}^\top \boldsymbol{\alpha} - \frac{\lambda \eta}{2} \|\mathbf{m}_\lambda(\boldsymbol{\alpha})_{\mathcal{F}}\|_2^2, \quad (10)$$

where $\mathbf{m}_{\mathcal{F}}$, $\mathbf{c}_{ij_{\mathcal{F}}}$, and $\mathbf{m}_\lambda(\boldsymbol{\alpha})_{\mathcal{F}}$ are sub-vectors specified by \mathcal{F} . If the size of \mathcal{F} is moderate, these sub-problems are significantly computationally easier to solve than the original problems.

We introduce several criteria that determine whether the feature k should be included in \mathcal{F} using the techniques of *safe screening* (Ghaoui et al., 2010) and *working set selection* (Fan et al., 2008). A general form of our criteria can be written as

$$\mathbf{C}_{k,:} \mathbf{q} + r \|\mathbf{C}_{k,:}\|_2 \leq T, \quad (11)$$

where $\mathbf{q} \in \mathbb{R}_+^{2nK}$, $r \geq 0$, and $T \in \mathbb{R}$ are constants that assume different values for each criterion. If this inequality holds for k , we exclude the k -th feature from \mathcal{F} . An important property is that although our algorithm only solves these small sub-problems, we can guarantee the optimality of the final solution, as shown later.

However, selecting \mathcal{F} itself is computationally expensive because the evaluation of (11) requires $O(n)$ computations for each k . Thus, we exploit a tree structure of graphs for determining \mathcal{F} . Figure 1 shows an example of such a tree, which can be constructed by a graph mining algorithm, such as gSpan (Yan and Han, 2002). Suppose that the k -th node corresponds to the k -th dimension of \mathbf{x} (note that the node index here is not the order of the visit). If a graph corresponding to the k -th node is a subgraph of the k' -th node, the node k' is a descendant of k , which is denoted as $k' \supseteq k$. Then, the following monotonic relation is immediately derived from the monotonicity of ϕ_H :

$$x_{i,k'} \leq x_{i,k} \text{ if } k' \supseteq k. \quad (12)$$

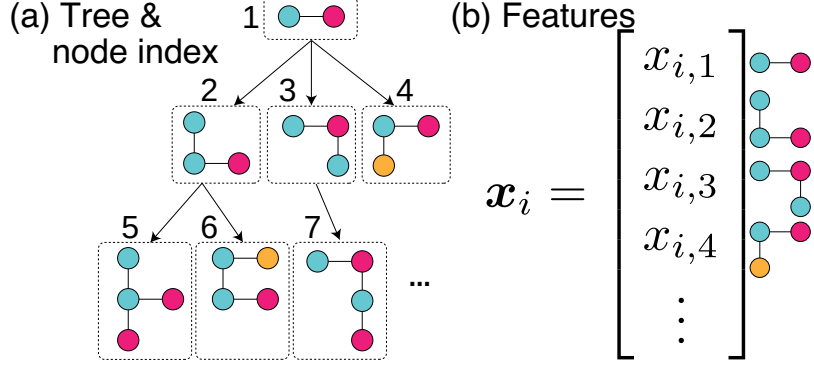


Figure 1: Schematic illustration of a tree and features.

Because any parent node is a subgraph of its children in the gSpan tree Figure 1, the non-overlapped frequency $\#(H \sqsubseteq G)$ of subgraph H in G is monotonically non-increasing while descending the tree node. Then, the condition (12) is obviously satisfied because for a sequence of $H \sqsubseteq H' \sqsubseteq H'' \sqsubseteq \dots$ in the descending path of the tree, $x_{i,k(H)} = \phi_H(G_i) = g(\#(H \sqsubseteq G))$ is monotonically non-increasing, where $x_{i,k(H)}$ is a feature corresponding to H in G_i . Based on this property, the following lemma enables us to prune a node during the tree traversal.

Lemma 4.1. *Let*

$$\text{Prune}(k|\mathbf{q}, r) := \sum_{i \in [n]} \sum_{l \in \mathcal{D}_i} q_{il} \max\{x_{i,k}, x_{l,k}\}^2 + r \sqrt{\sum_{i \in [n]} [\sum_{l \in \mathcal{D}_i} \max\{x_{i,k}, x_{l,k}\}^4 + \sum_{j \in \mathcal{S}_i} \max\{x_{i,k}, x_{j,k}\}^4]} \quad (13)$$

be a pruning criterion. Then, if the inequality

$$\text{Prune}(k|\mathbf{q}, r) \leq T \quad (14)$$

holds, for any descendant node $k' \supseteq k$, the following inequality holds:

$$\mathbf{C}_{k',:} \mathbf{q} + r \|\mathbf{C}_{k',:}\|_2 \leq T,$$

where $\mathbf{q} \in \mathbb{R}_+^{2nK}$ and $r \geq 0$ are an arbitrary constant vector and scalar variable, respectively.

This lemma indicates that if the condition (14) is satisfied, we can say that none of the descendant nodes are included in \mathcal{F} . Assuming that the indicator function $g(x) = 1_{x>0}$ is used in (2), a tighter bound can be obtained through the following lemma.

Lemma 4.2. *If $g(x) = 1_{x>0}$ is set in (2), the pruning criterion (13) can be replaced with*

$$\begin{aligned} \text{Prune}(k|\mathbf{q}, r) := & \sum_{i \in [n]} \max\left\{ \sum_{l \in \mathcal{D}_i} q_{il} x_{l,k}, x_{i,k} \left[\sum_{l \in \mathcal{D}_i} q_{il} - \sum_{j \in \mathcal{S}_i} q_{ij} (1 - x_{j,k}) \right] \right\} \\ & + r \sqrt{\sum_{i \in [n]} [\sum_{l \in \mathcal{D}_i} \max\{x_{i,k}, x_{l,k}\} + \sum_{j \in \mathcal{S}_i} \max\{x_{i,k}, x_{j,k}\}]}. \end{aligned}$$

By comparing the first terms of Lemmas 4.1 and 4.2, we see that Lemma 4.2 is tighter when $g(x) = 1_{x>0}$ as follows:

$$\begin{aligned} \sum_{i \in [n]} \max\left\{ \sum_{l \in \mathcal{D}_i} q_{il} x_{l,k}, x_{i,k} \left[\sum_{l \in \mathcal{D}_i} q_{il} - \sum_{j \in \mathcal{S}_i} q_{ij} (1 - x_{j,k}) \right] \right\} & \leq \sum_{i \in [n]} \max\left\{ \sum_{l \in \mathcal{D}_i} q_{il} x_{l,k}, x_{i,k} \sum_{l \in \mathcal{D}_i} q_{il} \right\} \\ & = \sum_{i \in [n]} \max\left\{ \sum_{l \in \mathcal{D}_i} q_{il} x_{l,k}, \sum_{l \in \mathcal{D}_i} q_{il} x_{i,k} \right\} \\ & \leq \sum_{i \in [n]} \sum_{l \in \mathcal{D}_i} \max\{q_{il} x_{l,k}, q_{il} x_{i,k}\} \\ & = \sum_{i \in [n]} \sum_{l \in \mathcal{D}_i} q_{il} \max\{x_{l,k}, x_{i,k}\}. \end{aligned}$$

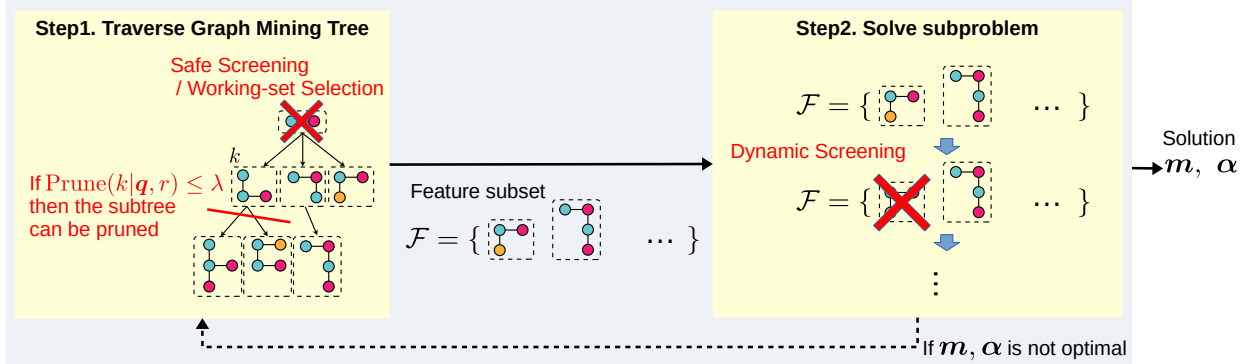


Figure 2: Schematic illustration of the optimization algorithm for IGML.

Table 1: Strategies to determine \mathcal{F} .

	Safe approaches based on the bounds in Sec. 4.1.1		Working set approaches (Sec. 4.2.1)
	Single λ (Sec. 4.1.2)	Range of λ (Sec. 4.1.3)	
For removing a single feature	Safe screening (SS) rule	Range-based safe screening (RSS)	Working set selection (WS)
For pruning a subtree	Safe pruning (SP) rule	Range-based safe pruning (RSP)	Working set pruning (WP)

A schematic illustration of the optimization algorithm for IGML is shown in Figure 2 (for further details, see Section 5). To generate a subset of features \mathcal{F} , we first traverse the graph mining tree during which the safe screening/working set selection procedure and their pruning extensions are performed (Step1). Next, we solve the sub-problem (9) with the generated \mathcal{F} using a standard gradient-based algorithm (Step2). Safe screening is also performed during the optimization iteration in Step2, which is referred to as *dynamic screening*. This further reduces the size of \mathcal{F} .

Before moving onto detailed formulations, we summarize our rules to determine \mathcal{F} in Table 1. The columns represent the different approaches to evaluating the necessity of features, i.e., safe and working set approaches. For the safe approaches, there are further ‘single λ ’ (described in Section 4.1.2) and ‘range of λ ’ (described in Section 4.1.3) approaches. The single λ approach considers safe rules for a specific λ , while the range of λ approach considers safe rules that can eliminate features for a range of λ (not just a specific value). Both the single and range approaches are based on the bounds of the region in which the optimal solution exists, for which details are given in Section 4.1.1. The rows of Table 1 indicate the variation of rules to remove one specific feature and rules to prune all features in a subtree.

4.1 Safe Screening

Safe screening (Ghaoui et al., 2010) was first proposed to identify unnecessary features in LASSO-type problems. Typically, this approach considers a bounded region of dual variables in which the optimal solution must exist. Then, we can eliminate dual inequality constraints that are never violated given that the solution exists in that region. The well-known Karush-Kuhn-Tucker (KKT) conditions show that this is equivalent to the elimination of primal variables that take value 0 at the optimal solution. In Section 4.1.1, we first derive a spherical bound for our optimal solution, and then in Section 4.1.2, a rule for safe screening is shown. Section 4.1.3 extends rules that are specifically useful for the regularization path calculation.

4.1.1 Sphere Bound for Optimal Solution

The following theorem provides a hyper-sphere containing the optimal dual variable α^* .

Theorem 4.1 (DGB). *For any pair of $\mathbf{m} \geq \mathbf{0}$ and $\alpha \geq \mathbf{0}$, the optimal dual variable α^* must satisfy*

$$\|\alpha - \alpha^*\|_2^2 \leq 4(P_\lambda(\mathbf{m}) - D_\lambda(\alpha)).$$

This bound is called the *duality gap bound* (DGB), and the parameters \mathbf{m} and α used to construct the bound are referred to as the *reference solution*. This inequality reveals that the optimal α^* should be in the inside of the sphere whose center is the reference solution α and radius is $2\sqrt{P_\lambda(\mathbf{m}) - D_\lambda(\alpha)}$, i.e., twice the square root of the duality gap. Therefore, if the quality of the reference solution \mathbf{m} and α is better, a tighter bound can be obtained. When the duality gap is zero, meaning that \mathbf{m} and α are optimal, the radius is shrunk to zero.

If the optimal solution for λ_0 is available as a reference solution to construct the bound for λ_1 , the following bound, called *regularization path bound* (RPB), can be obtained.

Theorem 4.2 (RPB). *Let α_0^* be the optimal solution for λ_0 and α_1^* be the optimal solution for λ_1 . Then,*

$$\left\| \alpha_1^* - \frac{\lambda_0 + \lambda_1}{2\lambda_0} \alpha_0^* \right\|_2^2 \leq \left\| \frac{\lambda_0 - \lambda_1}{2\lambda_0} \alpha_0^* \right\|_2^2.$$

This inequality indicates that the optimal dual solution for λ_1 (α_1^*) should be in the sphere whose center is $\frac{\lambda_0 + \lambda_1}{2\lambda_0} \alpha_0^*$ and radius is $\left\| \frac{\lambda_0 - \lambda_1}{2\lambda_0} \alpha_0^* \right\|_2$. However, RPB requires the exact solution, which is difficult to obtain in practice due to numerical errors. The *relaxed RPB* (RRPB) extends RPB to incorporate the approximate solution as a reference solution.

Theorem 4.3 (RRPB). *Assuming that α_0 satisfies $\|\alpha_0 - \alpha_0^*\|_2 \leq \epsilon$, the optimal solution α_1^* for λ_1 must satisfy*

$$\left\| \alpha_1^* - \frac{\lambda_0 + \lambda_1}{2\lambda_0} \alpha_0 \right\|_2 \leq \left\| \frac{\lambda_0 - \lambda_1}{2\lambda_0} \alpha_0 \right\|_2 + \left(\frac{\lambda_0 + \lambda_1}{2\lambda_0} + \frac{|\lambda_0 - \lambda_1|}{2\lambda_0} \right) \epsilon.$$

In Theorem 4.1, the reference α_0 is only assumed to be close to α_0^* within the radius ϵ instead of assuming that α_0^* is available. For example, ϵ can be obtained using the DGB (Theorem 4.1).

Similar bounds to those derived here were previously considered for the triplet screening of metric learning on usual numerical data (Yoshida et al., 2018, 2019b). Here, we extend a similar idea to derive subgraph screening.

4.1.2 Safe Screening and Safe Pruning Rules

Theorem 4.1 and 4.3 identify the regions where the optimal solution exists using a current feasible solution α . Further, from (6), when $\mathbf{C}_{k,:} \alpha^* \leq \lambda$, we have $m_k^* = 0$. This indicates that

$$\max_{\alpha \in \mathcal{B}} \mathbf{C}_{k,:} \alpha \leq \lambda \Rightarrow m_k^* = 0, \quad (15)$$

where \mathcal{B} is a region containing the optimal solution α^* , i.e., $\alpha^* \in \mathcal{B}$. As we derived in Section 4.1.1, the sphere-shaped \mathcal{B} can be constructed using feasible primal and dual solutions. By solving this maximization problem, we obtain the following safe screening (SS) rule.

Theorem 4.4 (SS Rule). *If the optimal solution α^* exists in the bound $\mathcal{B} = \{\alpha \mid \|\alpha - \mathbf{q}\|_2^2 \leq r^2\}$, the following rule holds*

$$\mathbf{C}_{k,:} \mathbf{q} + r \|\mathbf{C}_{k,:}\|_2 \leq \lambda \Rightarrow m_k^* = 0. \quad (16)$$

Theorem 4.4 indicates that we can eliminate unnecessary features by evaluating the condition shown in (16). Here, the theorem is written in a general form, and in practice, \mathbf{q} and r can be defined by the center and a radius of one of the sphere bounds, respectively. An important property of this rule is that it guarantees optimality, meaning that the sub-problems (9) and (10) have the exact same optimal solution to the original problem if \mathcal{F} is defined through this rule. However, it is still necessary to evaluate the rule for all p features, which is currently intractable. To avoid this problem, we derive a pruning strategy on the graph mining tree, which we call the safe pruning (SP) rule.

Theorem 4.5 (SP Rule). *If the optimal solution α^* is in the bound $\mathcal{B} = \{\alpha \mid \|\alpha - \mathbf{q}\|_2^2 \leq r^2, \mathbf{q} \geq \mathbf{0}\}$, the following rule holds*

$$\text{Prune}(k|\mathbf{q}, r) \leq \lambda \Rightarrow m_{k'}^* = 0, \text{ for } \forall k' \supseteq k. \quad (17)$$

This theorem is a direct consequence of Lemma 4.1. If this condition holds for a node k during the tree traversal, a subtree below that node can be pruned. This means that we can safely eliminate unnecessary subgraphs even without enumerating them. In this theorem, note that \mathcal{B} has an additional non-negative constraint $\mathbf{q} \geq \mathbf{0}$, but this is satisfied by all the bounds in Section 4.1.1 because of the non-negative constraint in the dual problem.

4.1.3 Range-based Safe Screening & Safe Pruning

The SS and SP rules apply to a fixed λ . The range-based extension identifies an interval of λ for which the satisfaction of SS/SP is guaranteed. This is particularly useful for the *path-wise optimization* or *regularization path* calculation, where the problem must be solved with a sequence of λ . We assume that the sequence is sorted in descending order, as optimization algorithms typically start from the trivial solution $\mathbf{m} = \mathbf{0}$. Let $\lambda = \lambda_1 \leq \lambda_0$. By combining RRPB with the rule (16), we obtain the following theorem.

Theorem 4.6 (Range-based Safe Screening (RSS)). *For any k , the following rule holds*

$$\lambda_a \leq \lambda \leq \lambda_0 \Rightarrow m_k^* = 0, \quad (18)$$

where

$$\lambda_a := \frac{\lambda_0(2\epsilon\|\mathbf{C}_{k,:}\|_2 + \|\alpha_0\|_2\|\mathbf{C}_{k,:}\|_2 + \mathbf{C}_{k,:}\alpha_0)}{2\lambda_0 + \|\alpha_0\|_2\|\mathbf{C}_{k,:}\|_2 - \mathbf{C}_{k,:}\alpha_0}.$$

This rule indicates that we can safely ignore m_k for $\lambda \in [\lambda_a, \lambda_0]$, while if $\lambda_a > \lambda_0$, the weight m_k cannot be removed by this rule. For SP, the range-based rule can also be derived from (17).

Theorem 4.7 (Range-based Safe Pruning (RSP)). *For any $k' \supseteq k$, the following pruning rule holds:*

$$\lambda'_a := \frac{\lambda_0(2\epsilon b + \|\alpha_0\|_2 b + a)}{2\lambda_0 + \|\alpha_0\|_2 b - a} \leq \lambda \leq \lambda_0 \Rightarrow m_{k'}^* = 0, \quad (19)$$

where

$$a := \sum_{i \in [n]} \sum_{l \in \mathcal{D}_i} \alpha_{0il} \max\{x_{l,k}, x_{i,k}\}^2,$$

$$b := \sqrt{\sum_{i \in [n]} [\sum_{l \in \mathcal{D}_i} \max\{x_{i,k}, x_{l,k}\}^4 + \sum_{j \in \mathcal{S}_i} \max\{x_{i,k}, x_{j,k}\}^4]}.$$

This theorem indicates that, while $\lambda \in [\lambda'_a, \lambda_0]$, we can safely remove the entire subtree of k . Analogously, if the feature vector is generated from $g(x) = 1_{x>0}$ (i.e., binary), the following theorem holds.

Theorem 4.8 (Range-Based Safe Pruning (RSP) for binary feature). *Assuming $g(x) = 1_{x>0}$ in (2), a and b in theorem 4.7 can be replaced with*

$$a := \sum_{i \in [n]} \max\left\{ \sum_{l \in \mathcal{D}_i} \alpha_{0il} x_{l,k}, x_{i,k} \left[\sum_{l \in \mathcal{D}_i} \alpha_{0il} - \sum_{j \in \mathcal{S}_i} \alpha_{0ij} (1 - x_{j,k}) \right] \right\},$$

$$b := \sqrt{\sum_{i \in [n]} \left[\sum_{l \in \mathcal{D}_i} \max\{x_{i,k}, x_{l,k}\} + \sum_{j \in \mathcal{S}_i} \max\{x_{i,k}, x_{j,k}\} \right]}.$$

Because these constants a and b are derived from the tighter bound in Lemma 4.2, the obtained range becomes wider than the range in Theorem 4.7.

Once we calculate λ_a and λ'_a of (18) and (19) for some λ , they are stored at each node of the tree. Subsequently, such λ_a and λ'_a can be used for the next tree traversal with different λ' . If the conditions of (18) or (19) are satisfied, the node can be skipped (RSS) or pruned (RSP). Otherwise, we update λ_a and λ'_a by using the current reference solution.

4.2 Working Set Method

Safe rules are strong rules in the sense that they can completely remove features; thus, they are sometimes too conservative to fully accelerate the optimization. In contrast, the *working set selection* is a widely accepted heuristic approach to selecting a subset of features.

4.2.1 Working Set Selection & Working Set Pruning

The working set (WS) method optimizes the problem with respect to only selected working set features. Then, if the optimality condition for the original problem is not satisfied, the working set is reselected and the optimization on the new working set restarts. This process iterates until optimality on the original problem is achieved.

Besides the safe rules, we use the following WS selection criterion, which is obtained directly from the KKT conditions:

$$\mathbf{C}_{k,:}\boldsymbol{\alpha} \leq \lambda. \quad (20)$$

If this inequality is satisfied, the k -th dimension is predicted as $m_k^* = 0$. Hence, the working set is defined by

$$\mathcal{W} := \{k \mid \mathbf{C}_{k,:}\boldsymbol{\alpha} > \lambda\}.$$

Although $m_i^* = 0$ for $i \notin \mathcal{W}$ is not guaranteed, the final convergence of the procedure is guaranteed by the following theorem.

Theorem 4.9 (Convergence of WS). *Assume that there is a solver for the sub-problem (9) (or equivalently (10)) that returns the optimal solution for given \mathcal{F} . The working set method, which iterates optimizing the sub-problem with $\mathcal{F} = \mathcal{W}$ and updating \mathcal{W} alternately, returns the optimal solution of the original problem in finite steps.*

However, here again, the inequality (20) needs to be evaluated for all features, which is computationally intractable.

The same pruning strategy as for SS/SP can be incorporated into working set selection. The criterion (20) is also a special case of (11), and Lemma 4.1 indicates that if the following inequality

$$\text{Prune}_{\text{WP}}(k) := \text{Prune}(k \mid \boldsymbol{\alpha}, 0) \leq \lambda,$$

holds, then no $k' \supseteq k$ is included in the working set. We refer to this criterion as working set pruning (WP).

4.2.2 Relation with Safe Rules

Note that for the working set method, we may need to update \mathcal{W} multiple times, unlike in the safe screening approaches, as shown by Theorem 4.9. Instead, the working set method can usually exclude a larger number of features compared with safe screening approaches. In fact, when the condition of the SS rule (16) is satisfied, the WS criterion (20) must likewise be satisfied. Because all the spheres (DGB, RPB and RRPB) contain the reference solution $\boldsymbol{\alpha}$, which is usually the current solution, the inequality

$$\mathbf{C}_{k,:}\boldsymbol{\alpha} \leq \max_{\boldsymbol{\alpha}' \in \mathcal{B}} \mathbf{C}_{k,:}\boldsymbol{\alpha}' \quad (21)$$

holds, where \mathcal{B} is a sphere created by DGB, RPB or RRPB. This indicates that when the SS rule excludes the k -th feature, the WS also excludes the k -th feature. However, to guarantee convergence, WS needs to be fixed until the sub-problem (9)–(10) is solved (Theorem 4.9). In contrast, the SS rule is applicable anytime during the optimization procedure without affecting the final optimality. This enables us to apply the SS rule even to the sub-problem (9)–(10), where \mathcal{F} is defined by WS as shown in Step 2 of Figure 2 (dynamic screening).

For the pruning rules, we first confirm the following two properties:

$$\begin{aligned} \text{Prune}(k \mid \mathbf{q}, r) &\geq \text{Prune}(k \mid \mathbf{q}, 0), \\ \text{Prune}(k \mid C\mathbf{q}, 0) &= C \text{Prune}(k \mid \mathbf{q}, 0), \end{aligned}$$

where $\mathbf{q} \in \mathbb{R}_+^{2nK}$ is the center of the sphere, $r \geq 0$ is the radius, and $C \in \mathbb{R}$ is a constant. In the case of DGB, the center of the sphere is the reference solution $\boldsymbol{\alpha}$ itself, i.e., $\mathbf{q} = \boldsymbol{\alpha}$. Then, the following relation holds between the SP criterion $\text{Prune}(k|\mathbf{q}, r)$ and WP criterion $\text{Prune}_{\text{WP}}(k)$:

$$\text{Prune}(k|\mathbf{q}, r) = \text{Prune}(k|\boldsymbol{\alpha}_0, r) \geq \text{Prune}(k|\boldsymbol{\alpha}_0, 0) = \text{Prune}_{\text{WP}}(k).$$

This once more indicates that when the SP rule is satisfied, the WP rule must be satisfied as well. When the RPB or RRPB sphere is used, the center of the sphere is $\mathbf{q} = \frac{\lambda_0 + \lambda_1}{2\lambda_0} \boldsymbol{\alpha}_0$. Assuming that the solution for λ_0 is used as the reference solution, i.e., $\boldsymbol{\alpha} = \boldsymbol{\alpha}_0$, we obtain

$$\begin{aligned} \text{Prune}(k|\mathbf{q}, r) &= \text{Prune}(k|\frac{\lambda_0 + \lambda_1}{2\lambda_0} \boldsymbol{\alpha}, r) \\ &\geq \text{Prune}(k|\frac{\lambda_0 + \lambda_1}{2\lambda_0} \boldsymbol{\alpha}, 0) \\ &= \frac{\lambda_0 + \lambda_1}{2\lambda_0} \text{Prune}(k|\boldsymbol{\alpha}, 0) \\ &= \frac{\lambda_0 + \lambda_1}{2\lambda_0} \text{Prune}_{\text{WP}}(k). \end{aligned}$$

Using this inequality, we obtain

$$\text{Prune}(k|\mathbf{q}, r) - \text{Prune}_{\text{WP}}(k) \geq \frac{\lambda_1 - \lambda_0}{2\lambda_0} \text{Prune}_{\text{WP}}(k).$$

From this inequality, if $\lambda_1 > \lambda_0$, then $\text{Prune}(k|\mathbf{q}, r) > \text{Prune}_{\text{WP}}(k)$ (note that $\text{Prune}_{\text{WP}}(k) \geq 0$ because $\boldsymbol{\alpha} \geq \mathbf{0}$), indicating that the pruning of WS is always tighter than that of the safe rule. However, in our algorithm presented in Section 5, $\lambda_1 < \lambda_0$ holds because we start from a larger value of λ and gradually decrease it. Then, this inequality does not hold, and $\text{Prune}(k|\mathbf{q}, r) < \text{Prune}_{\text{WP}}(k)$ becomes a possibility.

When the WS and WP rules are strictly tighter than the SS and SP rules, respectively, using both of WS/WP and SS/SP rules is equivalent to using WS/WP only (except for dynamic screening). Even in this case, the range-based safe approaches (the RSS and RSP rules) can still be effective. When the range-based rules are evaluated, we obtain the range of λ such that the SS or SP rule is satisfied. Thus, as long as λ is in that range, we do not need to evaluate any safe or working set rules.

5 Algorithm and Computations

5.1 Training with Path-wise Optimization

We employ *path-wise optimization* (Friedman et al., 2007), where the optimization starts from $\lambda = \lambda_{\max}$, which gradually decreases λ while optimizing \mathbf{m} . As can be seen from (8), λ_{\max} is defined by the maximum of the inner product $\mathbf{C}_{k,\cdot} \boldsymbol{\alpha}$. This value can also be found by a tree search with pruning. Suppose that we calculate $\mathbf{C}_{k,\cdot} \boldsymbol{\alpha}$ while traversing the tree and $\hat{\lambda}_{\max}$ is the current maximum value during the traversal. Using Lemma 4.1, we can derive the pruning rule

$$\text{Prune}(k|\boldsymbol{\alpha}, 0) \leq \hat{\lambda}_{\max}.$$

If this condition holds, the descendant nodes of k cannot be maximal, and thus we can identify λ_{\max} without calculating $\mathbf{C}_{k,\cdot} \boldsymbol{\alpha}$ for all candidate features.

Algorithm 1 shows the outer loop of our path-wise optimization. The TRAVERSE and SOLVE functions in Algorithm 1 are shown in Algorithm 2 and 3, respectively. Algorithm 1 first calculates λ_{\max} which is the minimum λ at which the optimal solution is $\mathbf{m}^* = \mathbf{0}$ (line 3). The outer loop in lines 5-14 is the process of decreasing λ with the decreasing rate R . The TRAVERSE function in line 7 determines the subset of features \mathcal{F} by traversing tree with SS and WS. The inner loop (line 9-13) alternately solves the optimization problem with the current \mathcal{F} and updates \mathcal{F} until the duality gap becomes less than the given threshold eps .

Algorithm 2 shows the TRAVERSE function, which recursively visits tree nodes to determine \mathcal{F} . The variable `node.pruning` contains λ'_a of RSP, and if the RSP condition (19) is satisfied (line 3), the function

Algorithm 1: Path-wise Optimization

```
1 function PATHWISEOPTIMIZATION( $R, T, \text{freq}, \text{MaxIter}, \text{eps}$ )
2    $\mathbf{m}_0 = \mathbf{0}, \boldsymbol{\alpha}_0 = [2L, \dots, 2L, 0, \dots, 0], \epsilon = 0$ 
3    $\lambda_0 = \lambda_{\max} = \max_k \mathbf{C}_{k,:} \boldsymbol{\alpha}_0$  ▷ compute  $\lambda_{\max}$ 
4   Initialize root node as root.children = empty, root.screening =  $\infty$ , and root.pruning =  $\infty$ 
5   for  $t \in \{1, 2, \dots, T\}$  do
6      $\lambda_t = R\lambda_{t-1}$ 
7      $\mathcal{F} = \text{TRAVERSE}(\lambda_{t-1}, \lambda_t, \boldsymbol{\alpha}_{t-1}, \epsilon, \text{root}, \text{true})$  ▷ get working set & update range of  $\lambda$ 
8      $\mathbf{m}_t = \mathbf{m}_{t-1}$ 
9     repeat
10       $\mathbf{m}_t, \boldsymbol{\alpha}_t, P = \text{SOLVE}(\lambda_t, \mathbf{m}_t, \mathcal{F}, \text{freq}, \text{MaxIter}, \text{eps})$ 
11       $\mathcal{F} = \text{TRAVERSE}(\text{null}, \lambda_t, \boldsymbol{\alpha}_t, \text{null}, \text{root}, \text{false})$  ▷ update working set
12       $\text{gap} = P - D_{\lambda_t}^{\mathcal{F}}(\boldsymbol{\alpha}_t)$ 
13      until  $\frac{\text{gap}}{P} \leq \text{eps}$  ▷ check optimality
14       $\epsilon = 2\sqrt{\text{gap}}$ 
15  return  $\{\mathbf{m}_t\}_{t=0}^{t=T}$ 
```

returns the current \mathcal{F} (the node is pruned). The variable `node.screening` contains λ_a of RSS, and if the RSS condition (18) is satisfied (line 5), this node can be skipped, and the function proceeds to the next node. If these two conditions are not satisfied, the function 1) updates `node.pruning` and `node.screening` if `update` is true, and 2) evaluates the conditions of RSP and WP (line 10), and RSS and WS (line 14). In lines 17-18, `gSpan` expands the children of the current node, and for each child node, the `TRAVERSE` function is called recursively.

Algorithm 3 shows a solver for the primal problem with the subset of features \mathcal{F} . Although we employ a simple projected gradient algorithm, any optimization algorithm can be used in this process. In lines 7-10, the SS rule is evaluated at every after `freq` iterations. Note that this SS is only for the sub-problems (9) and (10) created by the current \mathcal{F} (not for the original problems).

5.2 Enumerating Subgraphs for Test Data

To obtain a feature vector for test data, we only need to enumerate subgraphs with $m_k \neq 0$. When `gSpan` is used as a mining algorithm, a unique code, called *minimum DFS code*, is assigned to each node. If a DFS code for a node is (a_1, a_2, \dots, a_n) , a child node is represented by $(a_1, a_2, \dots, a_n, a_{n+1})$. This enables us to prune nodes that does not generate subgraphs with $m_k \neq 0$. Suppose that a subgraph $(a_1, a_2, a_3) = (x, y, z)$ must be enumerated, and that we are currently at node $(a_1) = (x)$. Then, a child with $(a_1, a_2) = (x, y)$ should be traversed, but a child with $(a_1, a_2) = (x, w)$ cannot generate (x, y, z) , and consequently we can stop the traversal of this node.

5.3 Post-processing

5.3.1 Learning Mahalanobis Distance for Selected Subgraphs

Instead of \mathbf{m} , the following Mahalanobis distance can be considered

$$d_{\mathbf{M}}(\mathbf{x}_i, \mathbf{x}_j) = (\mathbf{x}_i - \mathbf{x}_j)^\top \mathbf{M}(\mathbf{x}_i - \mathbf{x}_j), \quad (22)$$

where \mathbf{M} is a positive definite matrix. Directly optimizing \mathbf{M} requires $O(p^2)$ primal variables and semi-definite constraint, making the problem computationally expensive, even for relatively small p . Thus, as optional post-processing, we consider optimizing the Mahalanobis distance (22) for a small number of subgraphs selected by the optimized \mathbf{m} . Let $\mathcal{H} \subseteq \mathcal{G}$ be a set of subgraphs $m_{i(H)} > 0$ for $H \in \mathcal{H}$ and \mathbf{z}_i be a $h := |\mathcal{H}|$ dimensional feature vector consisting of $\phi_H(G_i)$ for $H \in \mathcal{H}$. For $\mathbf{M} \in \mathbb{R}^{h \times h}$, we consider the

Algorithm 2: Traverse gSpan with RSSP+WSP

```
1 function TRAVERSE( $\lambda_0, \lambda, \alpha_0, \epsilon, \text{node}, \text{update}$ )
2    $\mathcal{F} = \{\}, k = \text{node.feature}$ 
3   if  $\text{node.pruning} \leq \lambda$  then ▷ RSP rule
4     return  $\mathcal{F}$ 
5   else if  $\text{node.screening} \leq \lambda$  then ▷ RSS rule
6     do nothing
7   else ▷ update the range of  $\lambda$  if  $\text{update} = \text{true}$ 
8     if  $\text{update} = \text{true}$  then
9        $\text{node.pruning} = \frac{\lambda_0(2\epsilon b + \|\alpha_0\|_2 b + a)}{2\lambda_0 + \|\alpha_0\|_2 b - a}$  ▷ eq. (19)
10      if  $\text{node.pruning} \leq \lambda$  or  $\text{Prune}_{\text{WP}}(k) \leq \lambda$  then
11        return  $\mathcal{F}$ 
12      if  $\text{update} = \text{true}$  then
13         $\text{node.screening} = \frac{\lambda_0(2\epsilon \|\mathbf{C}_{k,:}\|_2 + \|\alpha_0\|_2 \|\mathbf{C}_{k,:}\|_2 + \mathbf{C}_{k,:}\alpha_0)}{2\lambda_0 + \|\alpha_0\|_2 \|\mathbf{C}_{k,:}\|_2 - \mathbf{C}_{k,:}\alpha_0}$  ▷ eq. (18)
14        if  $\text{node.screening} > \lambda$  and  $\mathbf{C}_{k,:}\alpha_0 > \lambda$  then
15           $\mathcal{F} = \mathcal{F} \cup \{k\}$ 
16      CREATECHILDREN( $\text{node}$ )
17      for  $\text{child} \in \text{node.children}$  do
18         $\mathcal{F} = \mathcal{F} \cup \text{TRAVERSE}(\lambda_0, \lambda, \alpha_0, \epsilon, \text{child}, \text{update})$ 
19      return  $\mathcal{F}$ 
20 function CREATECHILDREN( $\text{node}$ )
21   if  $\text{node.children} = \text{empty}$  then
22     Set  $\text{node.children}$  by gSpan
23   for  $\text{child} = \text{node.children}$  do
24      $\text{child.children} = \text{empty}$ 
25      $\text{child.screening} = \infty, \text{child.pruning} = \infty$ 
```

Algorithm 3: Gradient descent with dynamic screening

```
1 function SOLVE( $\lambda, \mathbf{m}, \mathcal{F}, \text{freq}, \text{MaxIter}, \text{eps}$ ) ▷ solve primal problem  $P_\lambda^{\mathcal{F}}$ , which is considered only
   for feature set  $\mathcal{F}$ 
2   for  $\text{iter} \in \{0, 1, \dots, \text{MaxIter}\}$  do
3     Compute  $\alpha$  by (7)
4      $\text{gap} = P_\lambda^{\mathcal{F}}(\mathbf{m}) - D_\lambda^{\mathcal{F}}(\alpha)$ 
5     if  $\frac{\text{gap}}{P_\lambda^{\mathcal{F}}(\mathbf{m})} \leq \text{eps}$  then ▷ convergence
6       return  $\mathbf{m}, \alpha, P_\lambda^{\mathcal{F}}(\mathbf{m})$ 
7     if  $\text{mod}(\text{iter}, \text{freq}) = 0$  then
8       for  $k \in \mathcal{F}$  do ▷ perform dynamic screening
9         if  $\|\mathbf{C}_{k,:}\alpha + 2\sqrt{\text{gap}}\|\mathbf{C}_{k,:}\|_2 \leq \lambda$  then ▷ SS by DGB
10           $\mathcal{F} = \mathcal{F} - \{k\}$ 
11         $\mathbf{m} = [\mathbf{m} - \gamma \nabla P_\lambda^{\mathcal{F}}(\mathbf{m})]_+$  ▷ update  $\mathbf{m}$  ( $\gamma$ : step-size)
12      return  $\mathbf{m}, \alpha, P_\lambda^{\mathcal{F}}(\mathbf{m})$ 
```

following metric learning problem:

$$\min_{\mathbf{M} \succeq \mathbf{O}} \sum_{i \in [n]} \left[\sum_{l \in \mathcal{D}_i} \ell_L(d_{\mathbf{M}}(\mathbf{z}_i, \mathbf{z}_l)) + \sum_{j \in \mathcal{S}_i} \ell_{-U}(-d_{\mathbf{M}}(\mathbf{z}_i, \mathbf{z}_j)) \right] + \lambda R(\mathbf{M}).$$

Above, $R: \mathbb{R}^{h \times h} \rightarrow \mathbb{R}$ is a regularization term for \mathbf{M} , where a typical setting is $R(\mathbf{M}) = \text{tr} \mathbf{M} + \frac{\eta}{2} \|\mathbf{M}\|_F^2$ with tr representing the trace of a matrix. This metric can be more discriminative, because it is optimized to the training data with a higher degree of freedom.

5.3.2 Vector Representation of a Graph

An explicit vector representation of an input graph can be obtained using optimized \mathbf{m} as follows:

$$\mathbf{x}'_i = \sqrt{\mathbf{m}} \circ \mathbf{x}_i \quad (23)$$

Unlike the original \mathbf{x}_i , the new representation \mathbf{x}'_i is computationally tractable because of the sparsity of \mathbf{m} , and simultaneously, this space should be highly discriminative. This property is beneficial for further analysis of the graph data. We show an example of applying the decision tree to the learned space later in the paper.

In the case of the general Mahalanobis distance given in Section 5.3.1, we can obtain further transformation. Let $\mathbf{M} = \mathbf{V} \mathbf{\Lambda} \mathbf{V}^\top$ be the eigenvalue decomposition of the learned \mathbf{M} . By employing the regularization term $R(\mathbf{M}) = \text{tr} \mathbf{M} + \frac{\eta}{2} \|\mathbf{M}\|_F^2$, some of the eigenvalues of \mathbf{M} can be shrunk to 0 because $\text{tr} \mathbf{M}$ is equal to the sum of the eigenvalues. If \mathbf{M} has $h' < h$ non-zero eigenvalues, $\mathbf{\Lambda}$ can be written as a $h' \times h'$ diagonal matrix, and \mathbf{V} is a $h \times h'$ matrix such that each column is the eigenvector of a non-zero eigenvalue. Then, a representation of the graph is

$$\sqrt{\mathbf{\Lambda}} \mathbf{V}^\top \mathbf{z}_i. \quad (24)$$

This can be considered as a supervised dimensionality reduction from h - to h' -dimensional space. Although each dimension no longer corresponds to a subgraph in this representation, the interpretation remains clear because each dimension of the transformed vector is simply a linear combination of \mathbf{z}_i .

6 Extensions

In this section, we consider three extensions of IGML: applications to other data types, employing a triplet loss function, and introducing vertex-label similarity.

6.1 Application to Other Structured Data

In addition to graph data, the proposed method can be applied to itemset/sequence data. For an itemset, the Jaccard index, defined as the size of the intersection of two sets divided by the size of the union, is the most popular similarity measure. Although a few studies have considered kernels for an itemset (Zhang et al., 2007), to the best of our knowledge, it remains difficult to adapt a metric on a given labeled dataset in an interpretable manner. In contrast, there are many kernel approaches for sequence data. The spectrum kernel (Leslie et al., 2001) creates a kernel matrix by enumerating all k -length subsequences in the given sequence. The mismatch kernel (Leslie et al., 2004) enumerates subsequences allowing m discrepancies in a pattern of length k . The gappy kernel (Leslie and Kuang, 2004; Kuksa et al., 2008) counts the number of k -mers (subsequences) with a certain number of gaps g that appear in the sequence. The above kernels require the value of hyperparameter k , although various lengths may in fact be related. The motif kernel (Zhang and Zaki, 2006; Pissis et al., 2013; Pissis, 2014) counts the number of ‘‘motifs’’ appearing in the input sequences, the ‘‘motif’’ must be decided by the user. Because these approaches are based on the idea of the ‘kernel’, they are unsupervised, unlike our approach.

By employing a similar approach to the graph input, we can construct a feature representation $\phi_H(X_i)$ for both itemset and sequence data. For the itemset data, the i -th input is a set of items $X_i \subseteq \mathcal{I}$, where \mathcal{I} is a set of all items, e.g., $X_1 = \{a, b\}$, $X_2 = \{b, c, e\}$, ... with the candidate items $\mathcal{I} = \{a, b, c, d, e\}$. The feature $\phi_H(X_i)$ is defined by $1_{H \subseteq X_i}$ for $\forall H \subseteq \mathcal{I}$. This feature $\phi_H(X_i)$ also has monotonicity $\phi_{H'}(X_i) \leq \phi_H(X_i)$ for

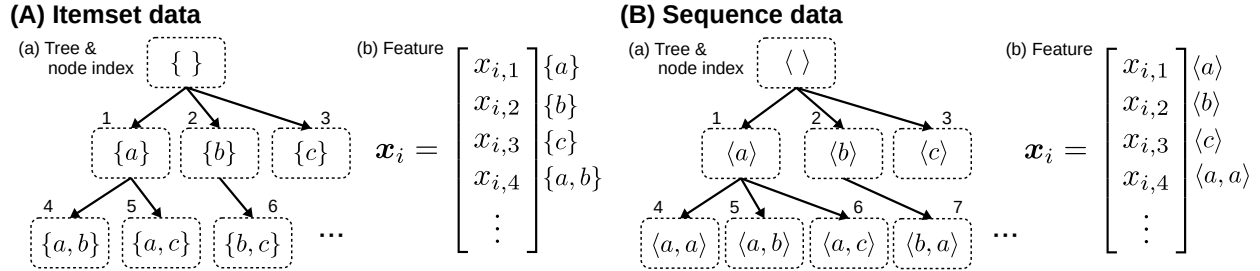


Figure 3: Schematic illustrations of trees and features for (A) itemset and (B) sequence data.

$H' \supseteq H$. In sequence data, the i -th input X_i is a sequence of items. Thus, the feature $\phi_H(X_i)$ is defined from the frequency of a sub-sequence H in the given X_i . For example, if we have $X_i = \langle b, b, a, b, a, c, d \rangle$ and $H = \langle b, a \rangle$, then H occurs twice in X_i . For sequence data, the monotonicity property is again guaranteed because $\phi_{H'}(X_i) \leq \phi_H(X_i)$, where H is a sub-sequence of H' . Because of these monotonicity properties, we can apply the same pruning procedures to both of itemset and sequence data. Figure 3 shows examples of trees that can be constructed by itemset and sequence mining algorithms (Agrawal et al., 1994; Pei et al., 2001).

6.2 Triplet Loss

We formulate the loss function of IGML as the pair-wise loss (3). Triplet loss functions are also widely used in metric learning (e.g., Weinberger and Saul, 2009):

$$\sum_{(i,j,l) \in \mathcal{T}} \ell_1(\mathbf{m}^\top \mathbf{c}_{il} - \mathbf{m}^\top \mathbf{c}_{ij}),$$

where \mathcal{T} is an index set of triplets consisting of (i, j, l) satisfying $y_i = y_j, y_i \neq y_l$. This loss incurs a penalty when the distance between samples in the same class is larger than the distance between samples in different classes. Because the loss is defined by a ‘triplet’ of samples, this approach can be more time-consuming than the pairwise approach. In contrast, the relative evaluation such as $d_m(\mathbf{x}_i, \mathbf{x}_j) < d_m(\mathbf{x}_i, \mathbf{x}_l)$ (the j -th sample must be closer to the i -th sample than the l -th sample) can capture the higher-order relations between input objects rather than penalizing the pair-wise distance.

A pruning rule can be derived even for the case of triplet loss. By defining $\mathbf{c}_{ijl} := \mathbf{c}_{il} - \mathbf{c}_{ij}$, the loss function can be written as

$$\sum_{(i,j,l) \in \mathcal{T}} \ell_1(\mathbf{m}^\top \mathbf{c}_{ijl}).$$

Because this has the same form as pairwise loss with $L = 1$ and $U = 0$, the optimization problem is reduced to the same form as the pairwise case. We require a slight modification of Lemma 4.1 because of the change of the constant coefficients (i.e., from \mathbf{c}_{ij} to \mathbf{c}_{ijl}). The equation (13) is changed to

$$\text{Prune}(k|\mathbf{q}, r) := \sum_{(i,j,l) \in \mathcal{T}} q_{ijl} \max\{x_{i,k}, x_{l,k}\}^2 + r \sqrt{\sum_{ijl} \max\{x_{i,k}, x_{l,k}\}^4}. \quad (25)$$

This is easily proven using

$$c_{ijl,k'} = (x_{i,k'} - x_{l,k'})^2 - (x_{i,k'} - x_{j,k'})^2 \leq \max\{x_{i,k}, x_{l,k}\}^2, \forall k' \supseteq k,$$

which is an immediate consequence of the monotonicity inequality (12).

6.3 Considering Vertex-Label Similarity

Because IGML is based on the exact matching of subgraphs to create the feature $\phi_H(G)$, it is difficult to provide a prediction for a graph that does not exactly match many of the selected subgraphs. Typically, this



Figure 4: Dissimilarity matrix among vertex-labels.

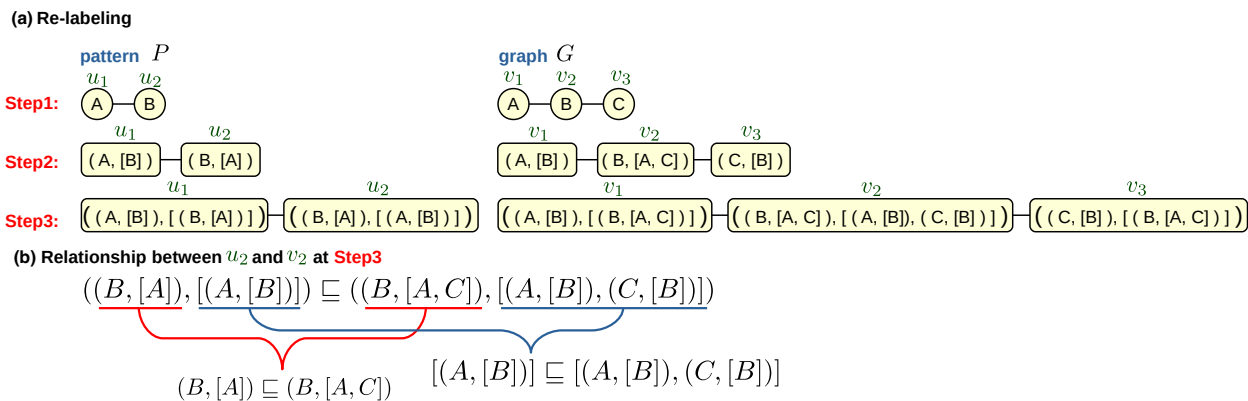


Figure 5: Re-labeling and inclusion relationship. $(X, [])$ is abbreviated as X , where $X \in \{A, B, C\}$. (a) In each step, all vertices are re-labeled by combining a vertex-label and neighboring labels at the previous step. (b) Example of inclusion relationship, defined by (26) and (27). The relation $L_P(u_2, 3) \sqsubseteq L_G(v_2, 3)$ is satisfied between u_2 and v_2 at Step3.

happens when the test dataset has a different distribution of vertex-labels. For example, in the case of the prediction on a chemical compound group whose atomic compositions are largely different from those in the training dataset, the exact match may not be expected as in the case of the training dataset. Therefore, we consider incorporating similarity/dissimilarity information of graph vertex-labels to relax this exact matching constraint. A toy example of vertex-label dissimilarity is shown in Figure 4. In this case, the ‘red’ vertex is similar to the ‘green’ vertex, while it is dissimilar to the ‘yellow’ vertex. For example, we can create this type of table by using prior domain knowledge (e.g., chemical properties of atoms). Even when no prior information is available, a similarity matrix can be inferred using any embedding method (e.g., Huang et al., 2017).

Because it is difficult to directly incorporate similarity information into our subgraph isomorphism-based feature $\phi_H(G)$, we first introduce a relaxed evaluation of inclusion of a graph P in a given graph G . We assume that P is obtained from the gSpan tree of the training data. Our approach is based on the idea of ‘re-labeling’ graph vertex-labels in the Weisfeiler-Lehman (WL) kernel (Shervashidze et al., 2011), which is a well-known graph kernel with an approximate graph isomorphism test. Figure 5 (a) shows an example of the re-labeling procedure, which is performed in a fixed number of recursive steps. The number of steps is denoted as T ($T = 3$ in the figure) and is assumed to be pre-specified. In step h , each graph vertex v has a level h hierarchical label $L_G(v, h) := (F^{(h)}, S^{(h)} = [S_1^{(h)}, \dots, S_n^{(h)}])$, where $F^{(h)}$ is recursively defined by the level $h - 1$ hierarchical label of the same vertex, i.e., $F^{(h)} = L_G(v, h - 1)$, and $S^{(h)}$ is a multiset created by the level $h - 1$ hierarchical labels $L_G(v', h - 1)$ from all neighboring vertices v' connected to v . Note that a multiset, denoted by $[\cdot, \cdot]$, is a set where duplicate elements are allowed. For example, in the graph G shown on the right side of Figure 5 (a), the hierarchical label of the vertex v_1 on level $h = 3$ is $L_G(v_1, 3) = ((A, [B]), [(B, [A, C])])$. In this case, $F^{(3)} = (A, [B])$, which is equal to $L_G(v_1, 2)$, and $S_1^{(3)} = (B, [A, C])$, which is equal to $L_G(v_2, 2)$. The original label A can also be regarded as a hierarchical label $(A, [])$ on the level $h = 1$, but it is shown as ‘ A ’ for simplicity.

We define a relation of the inclusion ‘ \sqsubseteq ’ between two hierarchical labels $L_P(u, h) = (F^{(h)}, S^{(h)} = [S_1^{(h)}, \dots, S_m^{(h)}])$ and $L_G(v, h) = (F'^{(h)}, S'^{(h)} = [S'_1^{(h)}, \dots, S'_n^{(h)}])$, which originate from the two vertices u and v in graphs P and G , respectively. We say that $L_P(v, h)$ is included in $L_G(u, h)$ and denote it by

$$L_P(v, h) \sqsubseteq L_G(u, h) \quad (26)$$

when the following recursive condition is satisfied:

$$\begin{cases} F^{(h)} = F'^{(h)}, & \text{if } S^{(h)} = S'^{(h)} = [], \\ F^{(h)} \sqsubseteq F'^{(h)} \wedge \exists \sigma (\wedge_{i \in [m]} S_i^{(h)} \sqsubseteq S'_{\sigma(i)}), & \text{otherwise,} \end{cases} \quad (27a)$$

$$\quad (27b)$$

where $\sigma : [m] \rightarrow [n]$ is an injection from $[m]$ to $[n]$ (i.e., $\sigma(i) \neq \sigma(j)$ when $i \neq j$), and $\exists \sigma (\wedge_{i \in [m]} S_i^{(h)} \sqsubseteq S'_{\sigma(i)})$ indicates that there exists an injection σ that satisfies $S_i^{(h)} \sqsubseteq S'_{\sigma(i)}$ for $\forall i \in [m]$. The first condition (27a) is for the case of $S^{(h)} = S'^{(h)} = []$, which occurs at the first level $h = 1$, and in this case, it simply evaluates whether the two hierarchical labels are equal, i.e., $F^{(h)} = F'^{(h)}$. Note that when $h = 1$, the hierarchical label is simply $(X, [])$, where X is one of the original vertex-labels. In the other case (27b), both of the two conditions $F^{(h)} \sqsubseteq F'^{(h)}$ and $\exists \sigma (\wedge_{i \in [m]} S_i^{(h)} \sqsubseteq S'_{\sigma(i)})$ are recursively defined. Suppose that we already evaluated the level $h - 1$ relation $L_P(u, h - 1) \sqsubseteq L_G(v, h - 1)$ for all pairs $\forall (u, v)$ from P and G . Because $F^{(h)} = L_P(u, h - 1)$ and $F'^{(h)} = L_G(v, h - 1)$, the condition $F^{(h)} \sqsubseteq F'^{(h)}$ is equivalent to $L_P(u, h - 1) \sqsubseteq L_G(v, h - 1)$, which is assumed to be already obtained on the level $h - 1$ computation. Because $S_i^{(h)}$ and $S'_i^{(h)}$ are also from hierarchical labels on level $h - 1$, the condition $\exists \sigma (\wedge_{i \in [m]} S_i^{(h)} \sqsubseteq S'_{\sigma(i)})$ is also recursive. From the result of the level $h - 1$ evaluations, we can determine whether $S_i^{(h)} \sqsubseteq S'_j^{(h)}$ holds for $\forall (i, j)$. Then, the evaluation of the condition $\exists \sigma (\wedge_{i \in [m]} S_i^{(h)} \sqsubseteq S'_{\sigma(i)})$ is reduced to a matching problem from $i \in [m]$ to $j \in [n]$. This problem can be simply transformed into a *maximum bipartite matching* problem for a pair of $\{S_1^{(h)}, \dots, S_m^{(h)}\}$ and $\{S'_1^{(h)}, \dots, S'_n^{(h)}\}$, where edges exist on a set of pairs $\{(i, j) \mid S_i^{(h)} \sqsubseteq S'_j^{(h)}\}$. When the maximum number of matchings is equal to m , this means that there exists an injection $\sigma(i)$ satisfying $\wedge_{i \in [m]} S_i^{(h)} \sqsubseteq S'_{\sigma(i)}$. It is well known that the maximum bipartite matching can be reduced to the *maximum flow problem*, which can be solved in the polynomial time (Goldberg and Tarjan, 1988). An example of the inclusion relationship is shown in Figure 5 (b).

Let $|P|$ and $|G|$ be the numbers of vertices in P and G , respectively. Then, multisets of the level T hierarchical labels of all the vertices in P and G are written as $[L_P(u_i, T)]_{i \in [|P|]} := [L_P(u_1, T), L_P(u_2, T), \dots, L_P(u_{|P|}, T)]$ and $[L_G(v_i, T)]_{i \in [|G|]} := [L_G(v_1, T), L_G(v_2, T), \dots, L_G(v_{|G|}, T)]$, respectively. For a feature of a given input graph G , we define the *approximate subgraph isomorphism feature (ASIF)* as follows:

$$x_{P \sqsubseteq G} := \begin{cases} 1, & \text{if } \exists \sigma (\wedge_{i \in [|P|]} L_P(u_i, T) \sqsubseteq L_G(v_{\sigma(i)}, T)), \\ 0, & \text{otherwise.} \end{cases} \quad (28)$$

This feature approximately evaluates the existence of a subgraph P in G using the level T hierarchical labels. ASIF satisfies the monotone decreasing property (12), i.e., $x_{P' \sqsubseteq G} \leq x_{P \sqsubseteq G}$ if $P' \supseteq P$, because the number of conditions in (27) only increases when P grows.

To incorporate label dissimilarity information (as shown in Figure 4) into ASIF, we first extend the label inclusion relation (26) by using the concept of *optimal transportation cost*. As a label similarity-based relaxed evaluation of $L_P(v, h) \sqsubseteq L_G(u, h)$, we define an asymmetric cost between $L_P(u, h)$ and $L_G(v, h)$ as follows

$$\begin{aligned} & \text{cost}_h(L_P(u, h) \rightarrow L_G(v, h)) \\ & := \begin{cases} \text{dissimilarity}(F^{(h)}, F'^{(h)}), & \text{if } S^{(h)} = S'^{(h)} = [], \\ \text{cost}_{h-1}(F^{(h)} \rightarrow F'^{(h)}) + \\ \quad \text{LTC}(S^{(h)} \rightarrow S'^{(h)}, \text{cost}_{h-1}), & \text{otherwise,} \end{cases} \end{aligned} \quad (29a)$$

$$\quad (29b)$$

where the second term of (29b) is

$$\text{LTC}(S^{(h)} \rightarrow S'^{(h)}, \text{cost}_{h-1}) := \min_{\sigma \in \mathcal{I}} \sum_{i \in [m]} \text{cost}_{h-1}(S_i^{(h)} \rightarrow S'_{\sigma(i)}), \quad (30)$$

which we refer to as the *label transportation cost* (LTC) representing the optimal transportation from the multiset $S^{(h)}$ to another multiset $S'^{(h)}$ among the set of all injections $\mathcal{I} := \{\forall \sigma : [m] \rightarrow [n] \mid \sigma(i) \neq \sigma(j) \text{ for } i \neq j\}$. The equation (29) has a recursive structure similar to that of (26). The first case (29a) occurs when $S^{(h)} = S'^{(h)} = []$, which is at the first level $h = 1$. In this case, cost_1 is defined by $\text{dissimilarity}(F^{(1)}, F'^{(1)})$, which is directly obtained as a dissimilarity between original labels since $F^{(1)}$ and $F'^{(1)}$ stem from the original vertex-labels. In the other case (29b), the cost is recursively defined as the sum of the cost from $F^{(h)}$ to $F'^{(h)}$ and the optimal-transport cost from $S^{(h)}$ to $S'^{(h)}$. Although this definition is recursive, as in the case of ASIF, the evaluation can be performed by computing sequentially from $h = 1$ to $h = T$. Because $F^{(h)} = L_P(v, h - 1)$ and $F'^{(h)} = L_G(u, h - 1)$, the first term $\text{cost}_{h-1}(F^{(h)} \rightarrow F'^{(h)})$ represents the cost between hierarchical labels on the level $h - 1$, which is assumed to already have been obtained. The second term $\text{LTC}(S^{(h)} \rightarrow S'^{(h)}, \text{cost}_{h-1})$ evaluates the best match between $[S_1^{(h)}, \dots, S_m^{(h)}]$ and $[S_1'^{(h)}, \dots, S_n'^{(h)}]$, as defined in (30). This matching problem can be seen as an optimal transportation problem, which minimizes the cost of the transportation of m items to n warehouses under the given cost matrix specified by cost_{h-1} . The values of cost_{h-1} for all the pairs in $[m]$ and $[n]$ are also available from the computation at the level $h - 1$. For the given cost values, the problem of $\text{LTC}(S^{(h)} \rightarrow S'^{(h)}, \text{cost}_{h-1})$ can be reduced to a *minimum-cost-flow problem* on a bipartite graph with a weight $\text{cost}_{h-1}(S_i^{(h)} \rightarrow S_j'^{(h)}, \text{cost}_{h-1})$ between $S_i^{(h)}$ and $S_j'^{(h)}$, which can be solved in polynomial time (Goldberg and Tarjan, 1988).

We define an asymmetric transport cost for two graphs P and G , which we call the *graph transportation cost* (GTC), as LTC from all level T hierarchical labels of P to those of G :

$$\text{GTC}(P \rightarrow G) := \text{LTC}([L_P(u_i, T)]_{i \in [|P|]} \rightarrow [L_G(v_i, T)]_{i \in [|G|]}, \text{cost}_T).$$

Then, as a feature of the input graph G , we define the following *sim-ASIF*:

$$x_{P \rightarrow G} := \exp\{-\rho \text{GTC}(P \rightarrow G)\}, \quad (31)$$

where $\rho > 0$ is a hyperparameter. This sim-ASIF can be regarded as a generalization of (28) based on the vertex-label similarity. When $\text{dissimilarity}(F^{(1)}, F'^{(1)}) := \infty \times 1_{F^{(1)} \neq F'^{(1)}}$, the feature (31) is equivalent to (28). Similarly to ASIF, $\text{GTC}(P \rightarrow G)$ satisfies the monotonicity property

$$\text{GTC}(P \rightarrow G) \leq \text{GTC}(P' \rightarrow G) \text{ for } P' \supseteq P$$

because the number of vertices to transport increases as P grows. Therefore, sim-ASIF (31) satisfies the monotonicity property, i.e., $x_{P' \rightarrow G} \leq x_{P \rightarrow G}$ if $P' \supseteq P$.

From the definition (31), sim-ASIF always has a positive value $x_{P \rightarrow G} > 0$ except when $\text{GTC}(P \rightarrow G) = \infty$, which may not be suitable for identifying a small number of important subgraphs. Further, in sim-ASIF, the bipartite graph in the minimum-cost-flow calculation $\text{LTC}(S \rightarrow S', \text{cost}_{h-1})$ is always a complete bipartite graph, where all vertices in S are connected to all vertices in S' . Because the efficiency of most of standard minimum-cost-flow algorithms depends on the number of edges, this may entail a large computational cost. As an extension to mitigate these issues, a threshold can be introduced into sim-ASIF as follows:

$$x := \begin{cases} \exp\{-\rho \text{GTC}(P \rightarrow G)\}, & \exp\{-\rho \text{GTC}(P \rightarrow G)\} > t \\ 0, & \exp\{-\rho \text{GTC}(P \rightarrow G)\} \leq t \end{cases}, \quad (32)$$

where $t > 0$ is a threshold parameter. In this definition, $x = 0$ when $\exp\{-\rho \text{GTC}(P \rightarrow G)\} \leq t$, i.e., $\text{GTC}(P \rightarrow G) \geq -(\log t)/\rho$. This indicates that if a cost is larger than $-(\log t)/\rho$, we can regard the cost as ∞ . Therefore, at any h , if the cost between $S_i^{(h)}$ and $S_j'^{(h)}$ is larger than $-(\log t)/\rho$, the edge between $S_i^{(h)}$ and $S_j'^{(h)}$ is not necessary. Then, the number of matching pairs can be less than m in $\text{LTC}(\cdot)$ because of the lack of edges, and in this case, the cost is regarded as ∞ . Furthermore, if $\text{cost}_h(F^{(h)} \rightarrow F'^{(h)})$ is larger than $-(\log t)/\rho$ in (29b), the computation of $\text{LTC}(S^{(h)} \rightarrow S'^{(h)}, \text{cost}_{h-1})$ is not required because $x = 0$ is determined.

Note that transportation-based graph metrics have been studied (e.g., Titouan et al., 2019), but the purpose of such studies was to evaluate the similarity between two graphs (not inclusion). Our (sim-)ASIF provides a feature with the monotonicity property as a natural relaxation of subgraph isomorphism, by which the optimality of our pruning strategy can be guaranteed. In contrast, there have been many studies on

inexact graph matching (Yan et al., 2016) such as eigenvector- (Leordeanu et al., 2012; Kang et al., 2013), edit distance- (Gao et al., 2010), and random walk-based (Gori et al., 2005; Cho et al., 2010) methods. Some of these methods provide a score for the matching, which can be seen as a similarity score between a searched graph pattern and a matched graph. However, they do not guarantee the monotonicity of the similarity score for pattern growth. If the similarity score satisfies monotonicity, it can be combined with IGML. Although we only consider vertex-labels, edge-labels can also be incorporated into (sim-)ASIF. A simple approach is to transform a labeled-edge into a labeled-node with two unlabeled edges, such that (sim-)ASIF is directly applicable.

7 Experiments

We evaluate the performance of IGML using the benchmark datasets shown in Table 3. These datasets are available from Kersting et al. (2016). We did not use edge labels because the implementations of compared methods cannot deal with them, and the maximum connected graph is used if the graph is not connected. Note that IGML currently cannot directly deal with continuous attributes, so we did not use them. A possible approach would be to perform discretization or quantization before the optimization, such as taking grid points or applying clustering in the attribute space. Building a more elaborated approach, such as dynamically determining discretization, is a possible future directions. The `#maxvertices` column in the table indicates the size (number of vertices) of the maximum subgraph considered in IGML. To fully identify important subgraphs, a large value of `#maxvertices` is preferred, but this can cause a correspondingly large memory requirement to store the gSpan tree. For each dataset, we set the largest value for which IGML could finish with a tractable amount memory. The sets \mathcal{S}_i and \mathcal{D}_i were selected as the ten nearest neighborhoods of \mathbf{x}_i ($K = |\mathcal{S}_i| = |\mathcal{D}_i| = 10$) by using the WL-Kernel. A sequence of the regularization coefficients was created by equally spacing 100 grid points on a logarithmic scale between λ_{\max} and $0.01\lambda_{\max}$. We set the minimum support in gSpan as 0, meaning that all the subgraphs in a given dataset were enumerated for as far as the graph satisfies the `#maxvertices` constraint. The gSpan tree is mainly traversed when the beginning of each λ as shown in Algorithm 1 (in the case of WS-based approaches, the tree is also traversed at every working set update). Note that the tree is dynamically constructed during this traversal without constructing the entire tree beforehand. In the working-set method, after convergence, it is necessary to traverse the tree again in order to confirm the overall optimality. If the termination condition is not satisfied, optimization with a new working set must be performed. The termination condition in the optimization is that the relative duality gap is less than 10^{-6} . In the experiment, we used $g(x) = 1_{x>0}$ in $\phi_H(G)$ with Lemma 4.2 unless otherwise noted. The dataset was randomly divided in such a way that the ratio of partitioning was train : validation : test = 0.6 : 0.2 : 0.2, and our experimental results were averaged over 10 runs.

7.1 Evaluating Computational Efficiency

In this section, we confirm the effect of the proposed pruning methods. We evaluated four settings: Safe Screening and Pruning: “SSP”, Range based Safe Screening and Pruning: “RSSP”, Working set Selection and Pruning: “WSP”, and the combination of WSP and RSSP: “WSP+RSSP”. Each method performed dynamic screening with DGB at every update of \mathbf{m} . We here used the AIDS dataset, where `#maxvertices`=30. In this dataset, when we fully traversed the gSpan tree without safe screening/working set selection, the number of tree nodes was more than 9.126×10^7 , at which point our implementation with gSpan stopped because we ran out of memory.

Figure 6 (a) shows the size of \mathcal{F} after the first traverse at each λ , and the number of non-zero m_k after the optimization is also shown as a baseline. We first observe that both approaches significantly reduced the number of features. Even for the largest case, where approximately 200 of features were finally selected by m_k , only less than 1000 features remained. We observe that WSP exhibited significantly smaller values than SSP. Instead, WSP may need to perform the entire tree search again because it cannot guarantee the sufficiency of the current \mathcal{F} , while SSP does not need to search the tree again because it guarantees that \mathcal{F} must contain all $m_k \neq 0$.

The number of visited nodes in the first traversal at each λ is shown in Figure 6 (b). Here, we added RSSP and WSP+RSSP, which are not shown in Figure 6 (a). Note that the `#remaining dimensions` is same

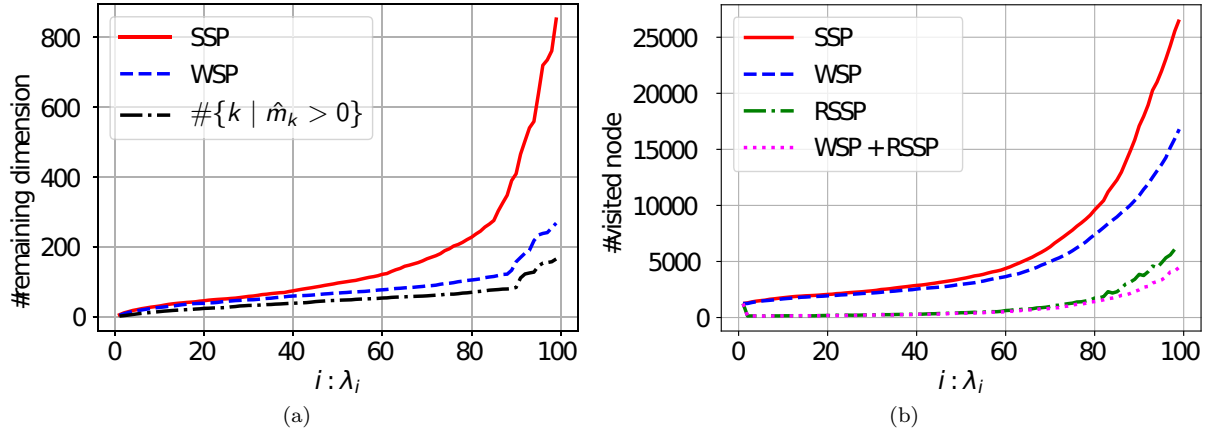


Figure 6: (a) Size of \mathcal{F} , and (b) number of visited nodes. Both were evaluated at the first traversal of each λ , where the index is shown on the horizontal axis. The dataset employed here was AIDS.

for SSP and RSSP, and for WSP and WSP+RSSP. Because RSSP is derived from SSP, it does not change the number of screened features. As we discussed in Section 4.2.2, WSP removes more features than RSSP, though it is not safe. We observed that the $\#\text{visited nodes}$ of SSP was the largest, but it was less than approximately 27000 ($27000/9.126 \times 10^7 \approx 0.0003$). Comparing SSP and WSP, we see that WSP pruned a larger number of nodes. In contrast, the $\#\text{visited nodes}$ of RSSP was less than 6000. The difference between SSP and RSSP indicates that a larger number of nodes can be skipped by the range-based method. Therefore, by combining the node skip by RSSP with the stronger pruning of WSP, the $\#\text{visited nodes}$ was further reduced. RSSP and WSP+RSSP had larger values at λ_0 than the subsequent λ_i . This is because of the effect of range-based screening and pruning. At λ_0 , every visited node in the tree calculates the ranges in which the screening and pruning rules are satisfied (i.e., RSS and RSP rules), and as a result, some nodes can be skipped during that λ_i is in those ranges. At every λ_i for $i > 0$, the ranges are updated only in the (non-skipped) visited nodes, and thus, the range-based rules take the effect except for λ_0 .

The total time of the path-wise optimization is shown in Table 2. RSSP and WSP+RSSP were fast with regard to the traversing time, and WSP and WSP+RSSP were fast with regard to the solving time. Note that because the tree is dynamically constructed during the traverse, the ‘Traverse’ time includes the time spent on the tree construction. In total, WSP+RSSP was the fastest. These results indicate that our method only took approximately 1 minute to solve the optimization problem with more than 9.126×10^7 variables. We also show the computational cost evaluation for other datasets in the Appendix I.

Although we have confirmed that IGML works efficiently on several benchmark datasets, completely elucidating general complexity of IGML remains as future work. The practical complexity at least depends on the graph size in the training data, $\#\text{maxvertices}$, $\#\text{samples}$, and the pruning rate. In terms of the graph size, traversing a large graph dataset using gSpan can be intractable because it requires all matched subgraphs to be maintained at each tree node. Therefore, applying IGML to large graphs, e.g., graphs with more than thousands of nodes, would be difficult. Meanwhile, the scalability of IGML depends not only on the sizes of graphs but also strongly on the performance of the pruning. However, we still do not have any general analytic complexity evaluation for the rate of the pruning that avoids exponential worst-case computations. In fact, we observed that there exist datasets in which efficiency of the pruning is not sufficient. For example, on the IMDB-BINARY and IMDB-MULTI datasets, which are also from (Kersting et al., 2016), a large number of small subgraphs are shared across all the different classes and instances (i.e., $x_{i,k} = 1$ for $\forall i$). Our upper bound in the pruning is based on the fact that $x_{i,k'} \leq x_{i,k}$ for descendant node k' in the mining tree. This bound becomes tighter when $x_{i,k} = 0$ for many i because 0 is the lower bound of $x_{i,k}$. In contrast, when many instances have $x_{i,k} = 1$, the bound can be loose, making traversal intractable. This is an important open problems common in predictive mining methods (Nakagawa et al., 2016; Morvan and Vert, 2018).

Table 2: Total time in path-wise optimization (sec) on AIDS dataset.

Method \ Process	Traverse	Solve	Total
SSP	25.9		112.7
	± 4.0	86.7	± 16.5
RSSP	7.7	± 14.1	94.4
	± 1.6		± 15.1
WSP	39.1		94.1
	± 3.7	55.0	± 11.6
WSP+	7.4	± 12.1	62.5
RSSP	± 1.1		± 12.3

7.2 Predictive Accuracy Comparison

In this section, we compare the prediction accuracy of IGML with those of the Graphlet-Kernel (GK)(Shervashidze et al., 2009), Shortest-Path Kernel (SPK)(Borgwardt and Kriegel, 2005), Random-Walk Kernel (RW)(Vishwanathan et al., 2010), Weisfeiler-Lehman Kernel (WL)(Shervashidze et al., 2011), and Deep Graph Convolutional Neural Network (DGCNN)(Zhang et al., 2018a). We used the implementations available at the URLs in the footnote¹. Note that we mainly compared methods for obtaining a metric between graphs. The graph kernel approach is one of most important existing approaches to defining a metric space of non-vector structured data. Although kernel functions are constructed in an un-supervised manner, their high prediction performance has been widely shown. In particular, the WL kernel is known for its comparable classification performance to recent graph neural networks (e.g., Niepert et al., 2016; Morris et al., 2019). Meanwhile, DGCNN can provide a vector representation of an input graph by using the outputs of some middle layer, which can be interpreted that a metric space is obtained through a supervised learning. We did not compare with (Saigo et al., 2009; Nakagawa et al., 2016; Morvan and Vert, 2018) as they only focused on specific linear prediction models rather than building a general discriminative space. We employed the k -nearest neighbors (k -nn) classifier to directly evaluate the discriminative ability of feature spaces constructed by IGML and each kernel function. We here employed the k -nn classifier for directly evaluating discriminative ability of feature spaces constructed by IGML and each kernel function. A graph kernel can be seen as an inner-product $k(G_i, G_j) = \langle \varphi(G_i), \varphi(G_j) \rangle$, where φ is a projection from a graph to reproducing kernel Hilbert space. Then, the distance can be written as $\|\varphi(G_i) - \varphi(G_j)\| = \sqrt{k(G_i, G_i) - 2K(G_i, G_j) + k(G_j, G_j)}$. The values of k for the k -nn were $k = 1, 3, 5, 7, \dots, 49$ and hyperparameters of each method were selected using the validation data, and the prediction accuracy was evaluated on the test data. The graphlet size for GK was set up to 6. The parameter λ_{RW} for RW was set to the recommended $\lambda_{RW} = \max_{i \in \mathbb{Z}: 10^i < 1/d^2} 10^i$, where d denotes the maximum degree. The loop parameter h of WL was selected from $0, 1, 2, \dots, 10$ by using the validation data. For DGCNN, the number of hidden units and their sort-pooling were also selected using the validation data, each ranging from 64, 128, 256 and from 40%, 60%, 80%, respectively.

The micro-F1 score for each dataset is shown in Table 3. "IGML (Diag)" indicates IGML with the weighted squared distance (1), and "IGML (Diag→Full)" indicates that with post-processing using the Mahalanobis distance (22). "IGML (Diag)" yielded the best or comparable to the best score on seven out of nine datasets. This result is impressive because IGML uses a much simpler metric than the other methods. Among the seven datasets, "IGML (Diag→Full)" slightly improved the mean accuracy on four datasets, but the difference was not significant. This may suggest that the diagonal weighting can have enough performance in many practical settings. WL kernel also exhibited superior performance, showing the best or comparable to the best accuracy on six datasets. DGCNN showed high accuracy with on the DBLP_v1 dataset, which has a large number of samples, while its accuracy was low for the other datasets.

7.3 Illustrative Examples of Selected Subgraphs

Figure 7 shows an illustrative example of IGML on the Mutagenicity dataset, where mutagenicity was predicted from a graph representation of molecules. Figure 7 (a) is a graphical representation of subgraphs, each of which has a weight shown in (b). For example, we can clearly see that subgraph #2 is estimated as an important sub-structure to discriminate different classes. Figure 7 (c) shows a heatmap of the transformation

¹<https://github.com/ysig/GraKeL> for GK, <http://mlcb.is.tuebingen.mpg.de/Mitarbeiter/Nino/Graphkernels/> for the other graph kernel, and https://github.com/muhanzhang/pytorch_DGCNN for DGCNN.

Table 3: Comparison of micro-F1 score. OOM means out of memory. “>1week” indicates that the algorithm ran for more than a week. The numbers after the “±” are the standard deviations. Every dataset had two classes. The bold font indicates the best average value and the ‘*’ symbol indicates that it is comparable to the best value in terms of one-sided t-test (significance level 0.05).

Method \ Dataset	AIDS	BZR	DD	DHFR	FRANKE NSTEIN	Mutag enicity	NCI1	COX2	DBLP_v1
#samples	2000	405	1178	467	4337	4337	4110	467	19456
#maxvertices	30	15	30	15	15	10	15	15	30
GK	0.967 ± 0.010	0.794 ± 0.036	0.700 ± 0.015	0.707 ± 0.034	0.628 ± 0.012	0.667 ± 0.010	0.640 ± 0.016	*0.781 ± 0.026	OOM
SPK	0.994 ± 0.003	*0.842 ± 0.039	>1week	0.737 ± 0.040	0.640 ± 0.012	0.719 ± 0.014	0.722 ± 0.012	*0.774 ± 0.034	0.784 ± 0.012
RW	0.998 ± 0.002	0.811 ± 0.025	OOM	0.659 ± 0.032	0.616 ± 0.013	0.679 ± 0.018	0.649 ± 0.017	*0.770 ± 0.038	OOM
WL	0.995 ± 0.003	*0.854 ± 0.039	*0.769 ± 0.027	*0.780 ± 0.045	*0.694 ± 0.017	0.768 ± 0.012	*0.772 ± 0.015	0.790 ± 0.040	0.814 ± 0.014
DGCNN	0.985 ± 0.005	0.791 ± 0.020	*0.773 ± 0.023	0.678 ± 0.030	0.615 ± 0.016	0.705 ± 0.018	0.706 ± 0.016	*0.764 ± 0.039	0.927 ± 0.003
IGML (Diag)	0.976 ± 0.006	0.860 ± 0.030	*0.778 ± 0.026	0.797 ± 0.035	*0.696 ± 0.014	*0.783 ± 0.016	*0.775 ± 0.012	*0.777 ± 0.037	0.860 ± 0.005
IGML (Diag→Full)	0.977 ± 0.008	0.830 ± 0.029	0.783 ± 0.022	*0.794 ± 0.042	0.699 ± 0.013	0.790 ± 0.023	0.782 ± 0.014	*0.773 ± 0.038	0.856 ± 0.005

matrix $\sqrt{\Lambda}\mathbf{V}^\top$ optimized for the thirteen features, containing three non-zero eigenvalues. For example, we see that the subgraphs of #10 and #12 have similar columns in the heatmap. This indicates that these two similar subgraphs (#10 contains #12) are shrunk to almost same representation by the regularization term $R(\mathbf{M})$.

As another example of graph data analysis on the learned representation, we applied the decision tree algorithm to the obtained feature (23) on the Mutagenicity dataset. Although there has been a study constructing a decision tree directly for graph data (Nguyen et al., 2006), it requires a severe restriction on the patterns to be considered for computational feasibility. In contrast, because (23) is a simple vector representation with a reasonable dimension, it is quite easy to apply the decision tree algorithm. We selected two paths from the obtained decision tree as shown in Figure 8. For example, in the path (a), if a given graph contains “ $O=N$ ”, and does not contain “ $H-O-C-C=C-C-H$ ”, and contains “ $N-C=C-C=C < \frac{C}{C}$ ”, the given graph is predicted as $y = 0$ with probability 140/146. Both rules clearly separate the two classes, which is highly insightful as we can trace the process of the decision based on the subgraphs.

7.4 Experiments for Three Extensions

In this section, we evaluate the performance of the three extensions of IGML described in Section 6.

First, we evaluated the performance of IGML on itemset and sequence data using the benchmark datasets shown in the first two rows of Table 4 and 5. These datasets can be obtained from (Dua and Graff, 2017) and (Chang and Lin, 2011), respectively. We set the maximum-pattern size considered by IGML as 30. Table 4 lists the micro-F1 scores on the itemset datasets. We used k -nn with the Jaccard similarity as a baseline, where k was selected using the validation set, as described in Section 7.2. The scores of both of IGML (Diag) and (Diag→Full) were superior to those of the Jaccard similarity on all datasets. Table 5 lists the micro-F1 scores on the sequence dataset. Although IGML (Diag) did not outperform the mismatch kernel (Leslie et al., 2004) for the promoters dataset, IGML (Diag→Full) achieved a higher F1-score than the kernel on all datasets. Figure 9 shows an illustrative example of sequences identified by IGML on the promoters dataset, where the task was to predict whether an input DNA sequence stems from a promoter region. Figure 9 (a) is a graphical representation of the sequence, and the corresponding weights are shown in (b). For example, the sub-sequence #1 in (a) can be considered as an important sub-sequence to discriminate different classes.

Second, we show the results of the triplet formulation described in Section 6.2. To create the triplet set \mathcal{T} , we followed the approach in Shen et al. (2014), where k neighborhoods in the same class \mathbf{x}_j and k neighborhoods in different classes \mathbf{x}_l were sampled for each \mathbf{x}_i ($k = 4$). Here, IGML with the pairwise loss is referred to as ‘IGML (Pairwise)’, and IGML with the triplet loss is referred to as ‘IGML (Triplet)’. Table 6 compares the micro-F1 scores of IGML (Pairwise) and IGML (Triplet). IGML (Triplet) showed higher F1-scores than IGML (Pairwise) on three of nine datasets, but it was not computable on the two

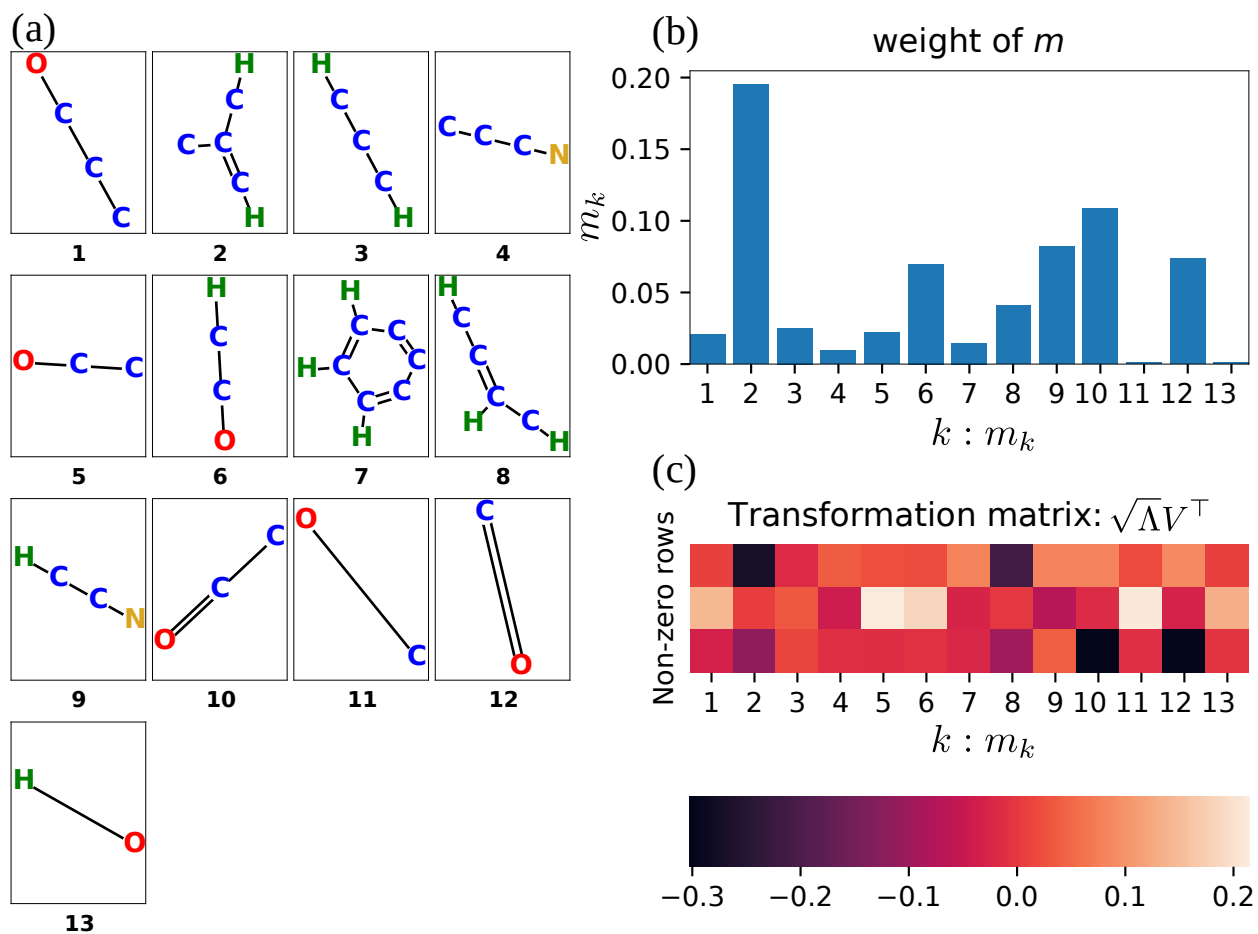


Figure 7: Examples of selected subgraphs. (a): Illustrations of subgraphs. (b): Learned weights of subgraphs. (c): Transformation matrix heatmap (24).

Table 4: Micro-F1 scores on itemset datasets.

Method \ Dataset	dna	car	nursery
#samples	2000	1728	12960
Jaccard Similarity	0.860±0.017	0.888±0.020	0.961±0.006
IGML (Diag)	0.908±0.014	0.936±0.011	0.982±0.005
IGML (Diag→Full)	0.931±0.009	0.948±0.014	0.993±0.002

Table 5: Micro-F1 scores on sequence datasets.

Method \ Dataset	promoters	splice
#samples	106	3190
Mismatch Kernel	0.832±0.081	0.596±0.017
IGML (Diag)	0.800±0.104	0.651±0.015
IGML (Diag→Full)	0.886±0.068	0.694±0.017

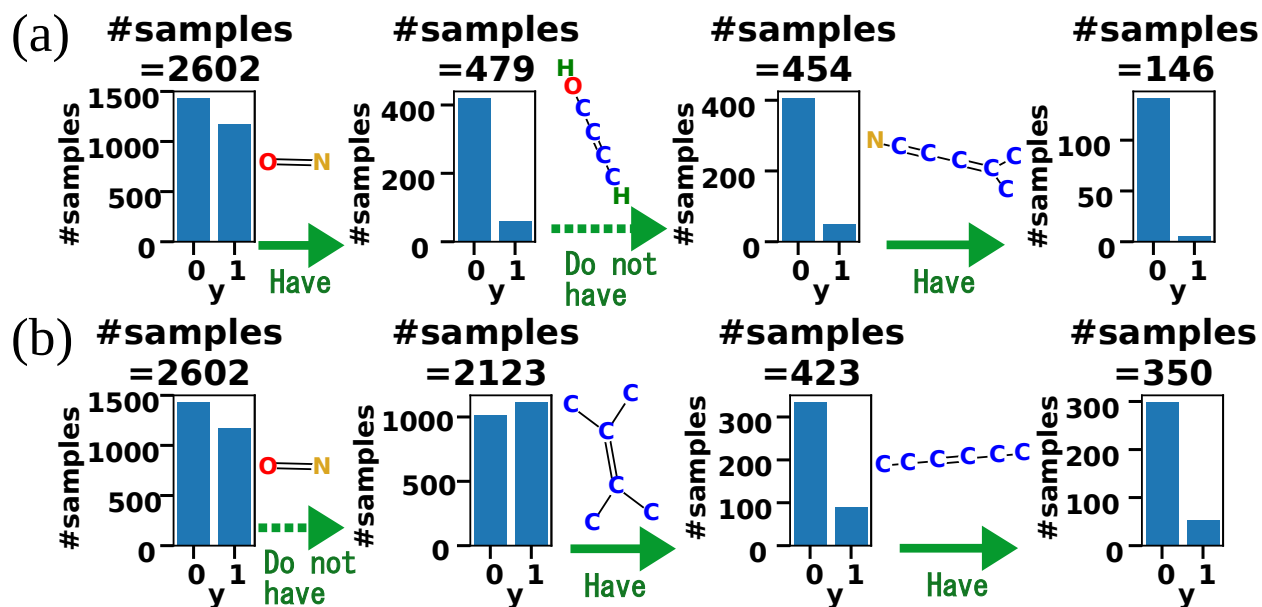


Figure 8: Examples of paths on decision tree constructed by selected subgraphs. #samples indicates the number of samples satisfying all preceding conditions.

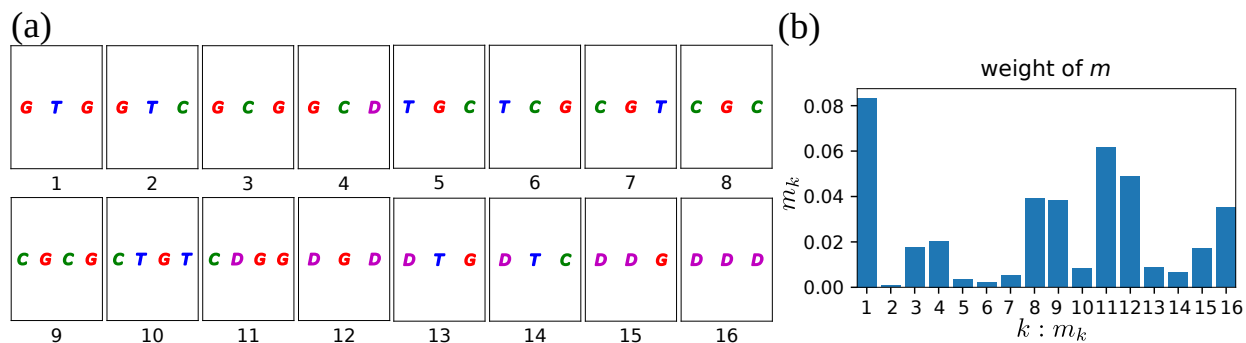


Figure 9: Examples of (a) selected sequences and (b) their weights for the promoters dataset.

Table 6: Comparison of IGML (Pairwise) and IGML (Triplet) in terms of micro-F1 score.

Method \ Dataset	AIDS	BZR	DD	DHFR	FRANKE NSTEIN	Mutag enicity	NCI1	COX2	DBLP_v1
IGML (Pairwise)	0.976	0.860	0.778	0.797	0.696	0.783	0.775	0.777	0.860
from Table 3	± 0.006	± 0.030	± 0.026	± 0.035	± 0.014	± 0.016	± 0.012	± 0.037	± 0.005
IGML (Triplet)	0.968	0.844	OOM	0.811	0.693	0.808	0.782	0.765	OOM
#maxvertices=10	± 0.012	± 0.032		± 0.033	± 0.013	± 0.012	± 0.013	± 0.042	

Table 7: Evaluation of sim-ASIF with micro-F1 score. The training and test sets of these datasets were split using a clustering algorithm such that the distribution of vertex-labels can be largely different.

#maxvertices	Feature \ Dataset	AIDS	Mutagenicity	NCI1
According to Table 3	Normal	0.574 \pm 0.039	0.720 \pm 0.014	0.735 \pm 0.025
8	Normal	0.572 \pm 0.038	0.705 \pm 0.017	0.726 \pm 0.019
8	sim-ASIF (32)	0.663 \pm 0.033	0.702 \pm 0.016	0.755 \pm 0.017

datasets due to running out of memory (OOM). This is because the pruning rule in the triplet case (25) was looser than in the pair-wise case.

Finally, we evaluated the sim-ASIF (32). We set the scaling factor of the exponential function as $\rho = 1$, the threshold of the feature as $t = 0.7$, and the number of re-labeling steps as $T = 3$. We employed a simple heuristic approach to create a dissimilarity matrix among vertex-labels using labeled graphs in the given dataset. Suppose that the set of possible vertex-labels is \mathcal{L} , and $f(\ell, \ell')$ is the frequency that $\ell \in \mathcal{L}$ and $\ell' \in \mathcal{L}$ are adjacent in all graphs of the dataset. By concatenating $f(\ell, \ell')$ for all $\ell' \in \mathcal{L}$, we obtained a vector representation of a label ℓ . We normalized this vector representation such that the vector had the unit L2 norm. By calculating the Euclidean distance of this normalized representations, we obtained the dissimilarity matrix of vertex-labels. We are particularly interested in the case where the distribution of the vertex-label frequency is largely different between the training and test datasets, because in this case the exact matching of IGML may not be suitable to provide a prediction. We synthetically emulated this setting by splitting the training and test datasets using a clustering algorithm. Each input graph was transformed into a vector created by the frequencies of each vertex-label $\ell \in \mathcal{L}$ contained in that graph. Subsequently, we applied the k -means clustering to split the dataset into two clusters, for which \mathcal{C}_1 and \mathcal{C}_2 denote sets of assigned data points, respectively. We used \mathcal{C}_1 for the training and validation datasets and \mathcal{C}_2 is used as the test dataset, where $|\mathcal{C}_1| \geq |\mathcal{C}_2|$. Following the same partitioning policy as in the above experiments, the size of the validation data was set as the same size of \mathcal{C}_2 , resulting from which the size of the training set was $|\mathcal{C}_1| - |\mathcal{C}_2|$. Table 7 lists the comparison of the micro-F1 scores on the AIDS, Mutagenicity, and NCI1 datasets. We did not consider other datasets as their training set sizes created from the above procedure were too small. We fixed the #maxvertices of sim-ASIF to 8, which was less than the value in our original IGML evaluation Table 3, because sim-ASIF takes more time than the feature without vertex-label similarity. For the original IGML, we show the result for the setting in Table 3 and the results with #maxvertices 8. IGML with sim-ASIF was superior to the original IGML for the both #maxvertices settings on the AIDS and NCI1 datasets, although it has smaller #maxvertices settings, as shown in Table 7. On the Mutagenicity dataset, sim-ASIF was inferior to the original IGML reported in Table 3, but in the comparison under the same #maxvertices value, their performances were comparable. These results suggest that when the exact matching of the subgraph is not appropriate, sim-ASIF can improve the prediction performance of IGML.

7.5 Performance on Frequency Feature

In this section, we evaluate IGML with $g(x) = \log(1 + x)$ instead of $g(x) = 1_{x>0}$. Note that because computing the frequency without overlapping $\#(H \sqsubseteq G)$ is NP-complete (Schreiber and Schwöbbermeyer, 2005), in addition to the exact count, we evaluated the feature defined by an upper bound of $\#(H \sqsubseteq G)$ (see Appendix J for details). We employed log because the scale of the frequency x is highly diversified. Based on the results in Section 7.1, we used WSP+RSSP in this section. The #maxvertices for each dataset followed those in Table 3.

The comparison of micro-F1 scores for the exact $\#(H \sqsubseteq G)$ and approximation of $\#(H \sqsubseteq G)$ is shown in Table 8. The exact $\#(H \sqsubseteq G)$ did not complete five datasets mainly due to the computational difficulty

Table 8: Micro-F1 scores for $g(x) = \log(1 + x)$.

Method \ Dataset	AIDS	BZR	DD	DHFR	FRANKE NSTEIN	Mutag enicity	NCI1	COX2	DBLP_v1
exact	-	0.833	-	0.802	-	-	-	0.769	0.858
$\#(H \sqsubseteq G)$		± 0.045		± 0.031				± 0.030	± 0.005
approximation	0.982	0.842	0.772	0.791	0.690	0.779	0.762	0.769	0.858
of $\#(H \sqsubseteq G)$	± 0.005	± 0.049	± 0.026	± 0.046	± 0.013	± 0.010	± 0.015	± 0.042	± 0.005

Table 9: Total time of path-wise optimization (sec) for $g(x) = \log(1 + x)$.

Dataset		AIDS			BZR		
Method \ Process		Traverse	Solve	Total	Traverse	Solve	Total
exact	$\#(H \sqsubseteq G)$		> a day		1662.2 \pm 93.0	93.0 \pm 19.4	1755.2 \pm 213.5
approximation	of $\#(H \sqsubseteq G)$	8.6 \pm 1.4	14.5 \pm 1.4	23.1 \pm 1.9	236.0 \pm 26.1	13.0 \pm 3.1	249.0 \pm 28.9

of the frequency counting. In contrast, the approximate $\#(H \sqsubseteq G)$ completed on all datasets. Overall, for both the exact and approximate frequency features, the micro-F1 scores were comparable with the case of $g(x) = 1_{x>0}$ shown in Table 3.

Table 9 lists the total times for the path-wise optimization for the exact $\#(H \sqsubseteq G)$ and the approximation of $\#(H \sqsubseteq G)$. On the AIDS dataset, the exact $\#(H \sqsubseteq G)$ did not complete within a day, while the traversal time using approximate $\#(H \sqsubseteq G)$ was only 8.6 sec. On the BZR dataset, the traversal time using the exact $\#(H \sqsubseteq G)$ was seven times that using the approximate $\#(H \sqsubseteq G)$. The solving time for the approximation was lower because $|\mathcal{F}|$ after traversing of the approximation was significantly less than that of the exact $\#(H \sqsubseteq G)$ in this case. Because the approximate $\#(H \sqsubseteq G)$ is an upper bound of the exact $\#(H \sqsubseteq G)$, the variation of the values of the exact $\#(H \sqsubseteq G)$ was smaller than the approximate $\#(H \sqsubseteq G)$. This resulted in higher correlations among features created by the exact $\#(H \sqsubseteq G)$. It is known that the elastic-net regularization tends to select correlated features simultaneously (Zou and Hastie, 2005), and therefore, $|\mathcal{F}|$ in the case of the exact $\#(H \sqsubseteq G)$ becomes larger than in the approximate case.

Figure 10 shows the number of visited nodes, size of the feature subset $|\mathcal{F}|$ after traversal, and the number of selected features on the AIDS dataset with the approximate $\#(H \sqsubseteq G)$. This indicates that IGML keeps the number of subgraphs tractable even if $g(x) = \log(1 + x)$ is used as the feature. The $\#$ -visited nodes was less than 3500, and $|\mathcal{F}|$ after traversal was sufficiently close to $|\{k \mid \hat{m}_k > 0\}|$. We see that $\#$ -visited nodes at λ_0 is larger than many subsequent λ_i s, and this is the effect of range-based rules, as shown in the case of Figure 6 (b).

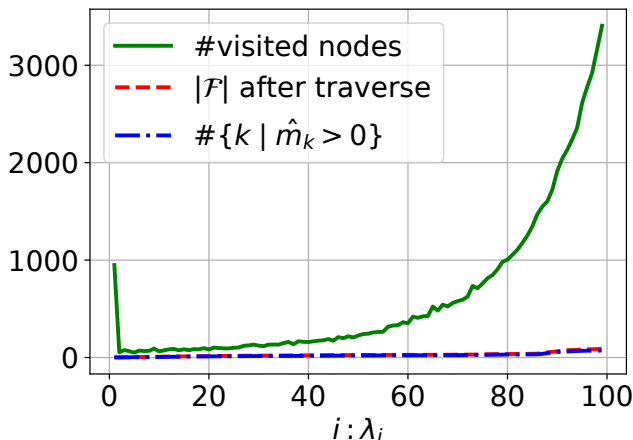


Figure 10: Results of IGML with $g(x) = \log(1 + x)$ on AIDS dataset.

8 Conclusions

In this paper, we proposed an interpretable metric learning method for graph data, named *interpretable graph metric learning* (IGML). To avoid computational difficulty, we built an optimization algorithm that combines safe screening, working set selection, and their pruning extensions. We also discussed the three extensions of IGML: (a) applications to other structured data, (b) triplet loss-based formulation, and (c) incorporating vertex-label similarity into the feature. We empirically evaluated the performance of IGML compared with existing graph classification methods. Although IGML was the only method with clear interpretability, it showed superior or comparable prediction performance compared to other state-of-the-art methods. The practicality of IGML was further demonstrated through some illustrative examples of identified subgraphs. Although IGML optimized the metric within tractable time in the experiments, the subgraphs were restricted to moderate sizes (up to 30), and a current major bottleneck for extracting larger-sized subgraphs is the memory requirement of the gSpan tree. Therefore, mitigating this memory consumption is an important future directions to apply IGML to a wider class of problems.

Funding

This work was supported by MEXT KAKENHI to I.T. (16H06538, 17H00758) and M.K. (16H06538, 17H04694); from JST CREST awarded to I.T. (JPMJCR1302, JPMJCR1502) and PRESTO awarded to M.K. (JPMJPR15N2); from the Collaborative Research Program of Institute for Chemical Research, Kyoto University to M.K. (grant #2018-33 and #2021-31); from the MI2I project of the Support Program for Starting Up Innovation Hub from JST awarded to I.T., and M.K.; and from RIKEN Center for AIP awarded to I.T.

Conflicts of interest/Competing interests

The authors declare no conflicts of interest.

Availability of data and material

All datasets used in the experiments are available on online (see Section 7 for details).

Code availability

The source code for the program used in the experiments is available at <https://github.com/takeuchi-lab/Learning-Interpretable-Metric-between-Graphs>.

References

- Adhikari, B., Zhang, Y., Ramakrishnan, N., and Prakash, B. A. (2018). Sub2vec: Feature learning for subgraphs. In *Pacific-Asia Conference on Knowledge Discovery and Data Mining*, pages 170–182. Springer.
- Agrawal, R., Srikant, R., et al. (1994). Fast algorithms for mining association rules. In *Proc. 20th int. conf. very large data bases, VLDB*, volume 1215, pages 487–499.
- Atwood, J. and Towsley, D. (2016). Diffusion-convolutional neural networks. In *Advances in Neural Information Processing Systems*, pages 1993–2001.
- Bellet, A., Habrard, A., and Sebban, M. (2012). Good edit similarity learning by loss minimization. *Machine Learning*, 89(1-2):5–35.
- Borgwardt, K. M. and Kriegel, H.-P. (2005). Shortest-path kernels on graphs. In *Proceedings of the Fifth IEEE International Conference on Data Mining (ICDM 2005)*, pages 74–81. IEEE Computer Society.

- Brinda, K. and Vishveshwara, S. (2005). A network representation of protein structures: Implications for protein stability. *Biophysical Journal*, 89(6):4159 – 4170.
- Chang, C.-C. and Lin, C.-J. (2011). LIBSVM: A library for support vector machines. *ACM Transactions on Intelligent Systems and Technology*, 2:27:1–27:27. Software available at <http://www.csie.ntu.edu.tw/~cjlin/libsvm>.
- Cheng, H., Yan, X., Han, J., and Philip, S. Y. (2008). Direct discriminative pattern mining for effective classification. In *2008 IEEE 24th International Conference on Data Engineering*, pages 169–178. IEEE.
- Cho, M., Lee, J., and Lee, K. M. (2010). Reweighted random walks for graph matching. In *European conference on Computer vision*, pages 492–505. Springer.
- Costa, F. and Grave, K. D. (2010). Fast neighborhood subgraph pairwise distance kernel. In *Proceedings of the 27th International Conference on International Conference on Machine Learning*, pages 255–262. Omnipress.
- Davis, J. V., Kulis, B., Jain, P., Sra, S., and Dhillon, I. S. (2007). Information-theoretic metric learning. In *Proceedings of the 24th international conference on Machine learning*, pages 209–216. ACM.
- Dua, D. and Graff, C. (2017). UCI machine learning repository. <http://archive.ics.uci.edu/ml>.
- Duvenaud, D. K., Maclaurin, D., Iparraguirre, J., Bombarell, R., Hirzel, T., Aspuru-Guzik, A., and Adams, R. P. (2015). Convolutional networks on graphs for learning molecular fingerprints. In *Advances in neural information processing systems*, pages 2224–2232. Curran Associates, Inc.
- Fan, R.-E., Chang, K.-W., Hsieh, C.-J., Wang, X.-R., and Lin, C.-J. (2008). LIBLINEAR: A library for large linear classification. *Journal of machine learning research*, 9:1871–1874.
- Feragen, A., Kasenburg, N., Petersen, J., de Bruijne, M., and Borgwardt, K. (2013). Scalable kernels for graphs with continuous attributes. In *Advances in Neural Information Processing Systems*, pages 216–224.
- Friedman, J., Hastie, T., Höfling, H., and Tibshirani, R. (2007). Pathwise coordinate optimization. *The Annals of Applied Statistics*, 1(2):302–332.
- Gao, X., Xiao, B., Tao, D., and Li, X. (2010). A survey of graph edit distance. *Pattern Analysis and applications*, 13(1):113–129.
- Gärtner, T., Flach, P., and Wrobel, S. (2003). On graph kernels: Hardness results and efficient alternatives. In *Learning Theory and Kernel Machines*, pages 129–143. Springer.
- Ghaoui, L. E., Viallon, V., and Rabbani, T. (2010). Safe feature elimination for the lasso and sparse supervised learning problems. *arXiv:1009.4219*.
- Goldberg, A. V. and Tarjan, R. E. (1988). A new approach to the maximum-flow problem. *Journal of the ACM (JACM)*, 35(4):921–940.
- Gori, M., Maggini, M., and Sarti, L. (2005). Exact and approximate graph matching using random walks. *IEEE transactions on pattern analysis and machine intelligence*, 27(7):1100–1111.
- Hsu, C.-W. and Lin, C.-J. (2002). A simple decomposition method for support vector machines. *Machine Learning*, 46(1):291–314.
- Huang, X., Li, J., and Hu, X. (2017). Label informed attributed network embedding. In *Proceedings of the Tenth ACM International Conference on Web Search and Data Mining*, pages 731–739.
- Kang, U., Hebert, M., and Park, S. (2013). Fast and scalable approximate spectral graph matching for correspondence problems. *Information Sciences*, 220:306–318.
- Kersting, K., Kriege, N. M., Morris, C., Mutzel, P., and Neumann, M. (2016). Benchmark data sets for graph kernels. <http://graphkernels.cs.tu-dortmund.de>.

- Kondor, R. and Borgwardt, K. M. (2008). The skew spectrum of graphs. In *Proceedings of the 25th international conference on Machine learning*, pages 496–503. ACM.
- Kondor, R. and Pan, H. (2016). The multiscale laplacian graph kernel. In *Advances in Neural Information Processing Systems*, pages 2990–2998.
- Kondor, R., Shervashidze, N., and Borgwardt, K. M. (2009). The graphlet spectrum. In *Proceedings of the 26th Annual International Conference on Machine Learning*, pages 529–536. ACM.
- Kriege, N. and Mutzel, P. (2012). Subgraph matching kernels for attributed graphs. *arXiv preprint arXiv:1206.6483*.
- Kuksa, P., Huang, P.-H., and Pavlovic, V. (2008). A fast, large-scale learning method for protein sequence classification. In *8th Int. Workshop on Data Mining in Bioinformatics*, pages 29–37.
- Lee, J. B., Rossi, R., and Kong, X. (2018). Graph classification using structural attention. In *Proceedings of the 24th ACM SIGKDD International Conference on Knowledge Discovery & Data Mining*, pages 1666–1674. ACM.
- Leordeanu, M., Sukthankar, R., and Hebert, M. (2012). Unsupervised learning for graph matching. *International journal of computer vision*, 96(1):28–45.
- Leslie, C., Eskin, E., and Noble, W. S. (2001). The spectrum kernel: A string kernel for svm protein classification. In *Biocomputing 2002*, pages 564–575. World Scientific.
- Leslie, C. and Kuang, R. (2004). Fast string kernels using inexact matching for protein sequences. *Journal of Machine Learning Research*, 5(Nov):1435–1455.
- Leslie, C. S., Eskin, E., Cohen, A., Weston, J., and Noble, W. S. (2004). Mismatch string kernels for discriminative protein classification. *Bioinformatics*, 20(4):467–476.
- Li, D. and Tian, Y. (2018). Survey and experimental study on metric learning methods. *Neural Networks*, 105:447–462.
- Morris, C., Kriege, N. M., Kersting, K., and Mutzel, P. (2016). Faster kernels for graphs with continuous attributes via hashing. In *Data Mining (ICDM), 2016 IEEE 16th International Conference on*, pages 1095–1100. IEEE.
- Morris, C., Ritzert, M., Fey, M., Hamilton, W. L., Lenssen, J. E., Rattan, G., and Grohe, M. (2019). Weisfeiler and leman go neural: Higher-order graph neural networks. In *The Thirty-Third AAAI Conference on Artificial Intelligence*, pages 4602–4609. AAAI Press.
- Morvan, M. L. and Vert, J.-P. (2018). WHInter: A working set algorithm for high-dimensional sparse second order interaction models. In *Proceedings of the 35th International Conference on Machine Learning*, volume 80, pages 3635–3644. PMLR.
- Nakagawa, K., Suzumura, S., Karasuyama, M., Tsuda, K., and Takeuchi, I. (2016). Safe pattern pruning: An efficient approach for predictive pattern mining. In *Proceedings of the 22nd ACM SIGKDD International Conference on Knowledge Discovery and Data Mining*, pages 1785–1794. ACM.
- Narayanan, A., Chandramohan, M., Venkatesan, R., Chen, L., Liu, Y., and Jaiswal, S. (2017). graph2vec: Learning distributed representations of graphs. *CoRR*, abs/1707.05005.
- Neuhaus, M. and Bunke, H. (2007). Automatic learning of cost functions for graph edit distance. *Information Sciences*, 177(1):239–247.
- Nguyen, P. C., Ohara, K., Mogi, A., Motoda, H., and Washio, T. (2006). Constructing decision trees for graph-structured data by chunkingless graph-based induction. In *Pacific-Asia Conference on Knowledge Discovery and Data Mining*, pages 390–399. Springer.

- Niepert, M., Ahmed, M., and Kutzkov, K. (2016). Learning convolutional neural networks for graphs. In *International conference on machine learning*, pages 2014–2023.
- Novak, P. K., Lavrač, N., and Webb, G. I. (2009). Supervised descriptive rule discovery: A unifying survey of contrast set, emerging pattern and subgroup mining. *Journal of Machine Learning Research*, 10:377–403.
- Orsini, F., Frasconi, P., and De Raedt, L. (2015). Graph invariant kernels. In *Proceedings of the Twenty-fourth International Joint Conference on Artificial Intelligence*, pages 3756–3762.
- Pei, J., Han, J., Mortazavi-Asl, B., Pinto, H., Chen, Q., Dayal, U., and Hsu, M.-C. (2001). Prefixspan: Mining sequential patterns efficiently by prefix-projected pattern growth. In *Proceedings 17th international conference on data engineering*, pages 215–224. IEEE.
- Pissis, S. P. (2014). Motex-ii: structured motif extraction from large-scale datasets. *BMC bioinformatics*, 15(1):235.
- Pissis, S. P., Stamatakis, A., and Pavlidis, P. (2013). Motex: A word-based hpc tool for motif extraction. In *Proceedings of the International Conference on Bioinformatics, Computational Biology and Biomedical Informatics*, page 13. ACM.
- Saigo, H., Nowozin, S., Kadowaki, T., Kudo, T., and Tsuda, K. (2009). gboost: a mathematical programming approach to graph classification and regression. *Machine Learning*, 75(1):69–89.
- Schreiber, F. and Schwöbbermeyer, H. (2005). Frequency concepts and pattern detection for the analysis of motifs in networks. In *Transactions on computational systems biology III*, pages 89–104. Springer.
- Shen, C., Kim, J., Liu, F., Wang, L., and Van Den Hengel, A. (2014). Efficient dual approach to distance metric learning. *IEEE transactions on neural networks and learning systems*, 25(2):394–406.
- Shervashidze, N. and Borgwardt, K. M. (2009). Fast subtree kernels on graphs. In *Advances in neural information processing systems*, pages 1660–1668.
- Shervashidze, N., Schweitzer, P., Leeuwen, E. J. v., Mehlhorn, K., and Borgwardt, K. M. (2011). Weisfeiler-lehman graph kernels. *Journal of Machine Learning Research*, 12(Sep):2539–2561.
- Shervashidze, N., Vishwanathan, S., Petri, T., Mehlhorn, K., and Borgwardt, K. (2009). Efficient graphlet kernels for large graph comparison. In *Artificial Intelligence and Statistics*, pages 488–495.
- Simonovsky, M. and Komodakis, N. (2017). Dynamic edge-conditioned filters in convolutional neural networks on graphs. In *Proc. CVPR*.
- Su, Y., Han, F., Harang, R. E., and Yan, X. (2016). A fast kernel for attributed graphs. In *Proceedings of the 2016 SIAM International Conference on Data Mining*, pages 486–494. SIAM.
- Sugiyama, M. and Borgwardt, K. (2015). Halting in random walk kernels. In *Advances in neural information processing systems*, pages 1639–1647.
- Takeuchi, I. and Sugiyama, M. (2011). Target neighbor consistent feature weighting for nearest neighbor classification. In *Advances in Neural Information Processing Systems*, volume 24, pages 576–584. Curran Associates, Inc.
- Thoma, M., Cheng, H., Gretton, A., Han, J., Kriegel, H.-P., Smola, A., Song, L., Yu, P. S., Yan, X., and Borgwardt, K. M. (2010). Discriminative frequent subgraph mining with optimality guarantees. *Statistical Analysis and Data Mining: The ASA Data Science Journal*, 3(5):302–318.
- Titouan, V., Courty, N., Tavenard, R., Laetitia, C., and Flamary, R. (2019). Optimal transport for structured data with application on graphs. In *Proceedings of the 36th International Conference on Machine Learning*, volume 97, pages 6275–6284. PMLR.
- Tixier, A. J.-P., Nikolentzos, G., Meladianos, P., and Vazirgiannis, M. (2018). Graph classification with 2d convolutional neural networks.

- Verma, S. and Zhang, Z.-L. (2017). Hunt for the unique, stable, sparse and fast feature learning on graphs. In *Advances in Neural Information Processing Systems*, pages 88–98.
- Vishwanathan, S. V. N., Schraudolph, N. N., Kondor, R., and Borgwardt, K. M. (2010). Graph kernels. *Journal of Machine Learning Research*, 11(Apr):1201–1242.
- Weinberger, K. Q. and Saul, L. K. (2009). Distance metric learning for large margin nearest neighbor classification. *Journal of Machine Learning Research*, 10(Feb):207–244.
- Xie, T. and Grossman, J. C. (2018). Crystal graph convolutional neural networks for an accurate and interpretable prediction of material properties. *Phys. Rev. Lett.*, 120:145301.
- Yan, J., Yin, X.-C., Lin, W., Deng, C., Zha, H., and Yang, X. (2016). A short survey of recent advances in graph matching. In *Proceedings of the 2016 ACM on International Conference on Multimedia Retrieval*, pages 167–174.
- Yan, X. and Han, J. (2002). gspan: Graph-based substructure pattern mining. In *Data Mining, 2002. ICDM 2003. Proceedings. 2002 IEEE International Conference on*, pages 721–724. IEEE.
- Yanardag, P. and Vishwanathan, S. (2015). Deep graph kernels. In *Proceedings of the 21th ACM SIGKDD International Conference on Knowledge Discovery and Data Mining*, pages 1365–1374. ACM.
- Yoshida, T., Takeuchi, I., and Karasuyama, M. (2018). Safe triplet screening for distance metric learning. In *Proceedings of the 24th ACM SIGKDD International Conference on Knowledge Discovery and Data Mining*, pages 2653–2662.
- Yoshida, T., Takeuchi, I., and Karasuyama, M. (2019a). Learning interpretable metric between graphs: Convex formulation and computation with graph mining. In *Proceedings of the 25th ACM SIGKDD International Conference on Knowledge Discovery and Data Mining*, pages 1026–1036.
- Yoshida, T., Takeuchi, I., and Karasuyama, M. (2019b). Safe triplet screening for distance metric learning. *Neural Computation*, 31(12):2432–2491.
- Zhang, M., Cui, Z., Neumann, M., and Chen, Y. (2018a). An end-to-end deep learning architecture for graph classification. In *Proceedings of AAAI Conference on Artificial Intelligence*.
- Zhang, Y., Liu, Y., Jing, X., and Yan, J. (2007). ACIK: association classifier based on itemset kernel. In *International Conference on Industrial, Engineering and Other Applications of Applied Intelligent Systems*, pages 865–875. Springer.
- Zhang, Y. and Zaki, M. J. (2006). Exmotif: efficient structured motif extraction. *Algorithms for Molecular Biology*, 1(1):21.
- Zhang, Z., Wang, M., Xiang, Y., Huang, Y., and Nehorai, A. (2018b). Retgk: Graph kernels based on return probabilities of random walks. In *Advances in Neural Information Processing Systems*, pages 3968–3978.
- Zou, H. and Hastie, T. (2005). Regularization and variable selection via the elastic net. *Journal of the royal statistical society: series B (statistical methodology)*, 67(2):301–320.

Appendix

A Dual Problem

The primal problem (4) can be re-written as

$$\begin{aligned} \min_{\mathbf{m}, \mathbf{z}} \quad & \sum_{i \in [n]} \left[\sum_{l \in \mathcal{D}_i} \ell_L(z_{il}) + \sum_{j \in \mathcal{S}_i} \ell_{-U}(z_{ij}) \right] + \lambda R(\mathbf{m}) \\ \text{s.t.} \quad & \mathbf{m} \geq \mathbf{0}, z_{il} = \mathbf{m}^\top \mathbf{c}_{il}, z_{ij} = -\mathbf{m}^\top \mathbf{c}_{ij}. \end{aligned}$$

The Lagrange function \mathcal{L} is

$$\begin{aligned} \mathcal{L}(\mathbf{m}, \mathbf{z}, \boldsymbol{\alpha}, \boldsymbol{\beta}) := & \sum_{i \in [n]} \left[\sum_{l \in \mathcal{D}_i} \ell_L(z_{il}) + \sum_{j \in \mathcal{S}_i} \ell_{-U}(z_{ij}) \right] + \lambda R(\mathbf{m}) \\ & + \sum_{i \in [n]} \left[\sum_{l \in \mathcal{D}_i} \alpha_{il} (z_{il} - \mathbf{m}^\top \mathbf{c}_{il}) + \sum_{j \in \mathcal{S}_i} \alpha_{ij} (z_{ij} + \mathbf{m}^\top \mathbf{c}_{ij}) \right] - \boldsymbol{\beta}^\top \mathbf{m}, \end{aligned}$$

where $\boldsymbol{\alpha} \in \mathbb{R}^{2nK}$ and $\boldsymbol{\beta} \in \mathbb{R}_+^p$ are Lagrange multipliers. The dual function D_λ is then

$$D_\lambda(\boldsymbol{\alpha}, \boldsymbol{\beta}) := \inf_{\mathbf{m}, \mathbf{z}} \mathcal{L}(\mathbf{m}, \mathbf{z}, \boldsymbol{\alpha}, \boldsymbol{\beta}). \quad (33)$$

By the definition of the dual function in (33), to minimize \mathcal{L} with respect to \mathbf{m} , by partially differentiating \mathcal{L} , we obtain

$$\nabla_{\mathbf{m}} \mathcal{L} = \lambda(\mathbf{1} + \boldsymbol{\eta} \mathbf{m}) + \sum_{i \in [n]} \left[- \sum_{l \in \mathcal{D}_i} \alpha_{il} \mathbf{c}_{il} + \sum_{j \in \mathcal{S}_i} \alpha_{ij} \mathbf{c}_{ij} \right] - \boldsymbol{\beta} = \mathbf{0}. \quad (34)$$

The convex conjugate function of ℓ_t is

$$\ell_t^*(-\alpha_{ij}) = \sup_{z_{ij}} \{(-\alpha_{ij})z_{ij} - \ell_t(z_{ij})\}, \quad (35)$$

which can be written as

$$\ell_t^*(x_*) = \frac{1}{4}x_*^2 + tx_*, (x_* \leq 0). \quad (36)$$

From (34), (35), and (36), the dual function can be written as

$$\begin{aligned} D_\lambda(\boldsymbol{\alpha}, \boldsymbol{\beta}) &= - \sum_{i \in [n]} \left[\sum_{l \in \mathcal{D}_i} \ell_L^*(-\alpha_{il}) + \sum_{j \in \mathcal{S}_i} \ell_{-U}^*(-\alpha_{ij}) \right] - \frac{\lambda \eta}{2} \|\mathbf{m}_\lambda(\boldsymbol{\alpha}, \boldsymbol{\beta})\|_2^2 \\ &= -\frac{1}{4} \|\boldsymbol{\alpha}\|_2^2 + \mathbf{t}^\top \boldsymbol{\alpha} - \frac{\lambda \eta}{2} \|\mathbf{m}_\lambda(\boldsymbol{\alpha}, \boldsymbol{\beta})\|_2^2. \end{aligned}$$

where

$$\begin{aligned} \mathbf{m}_\lambda(\boldsymbol{\alpha}, \boldsymbol{\beta}) &:= \frac{1}{\lambda \eta} \left[\boldsymbol{\beta} + \sum_{i \in [n]} \left(\sum_{l \in \mathcal{D}_i} \alpha_{il} \mathbf{c}_{il} - \sum_{j \in \mathcal{S}_i} \alpha_{ij} \mathbf{c}_{ij} \right) - \lambda \mathbf{1} \right] \\ &= \frac{1}{\lambda \eta} [\boldsymbol{\beta} + \mathbf{C} \boldsymbol{\alpha} - \lambda \mathbf{1}]. \end{aligned}$$

Therefore, although the dual problem can be written as

$$\max_{\boldsymbol{\alpha} \geq \mathbf{0}, \boldsymbol{\beta} \geq \mathbf{0}} D(\boldsymbol{\alpha}, \boldsymbol{\beta}),$$

by maximizing $D(\boldsymbol{\alpha}, \boldsymbol{\beta})$ with respect to $\boldsymbol{\beta}$, we obtain a more straightforward dual problem (5).

We obtain $\alpha_{ij} = -\ell'_t(z_{ij})$, used in (7), from the derivative of \mathcal{L} with respect to z_{ij} .

B Proof of Lemma 4.1

From (12), the value of $(x_{i,k'} - x_{j,k'})^2$ is bounded as follows:

$$\begin{aligned} (x_{i,k'} - x_{j,k'})^2 &\leq \max_{0 \leq x_{i,k'} \leq x_{i,k}, 0 \leq x_{j,k'} \leq x_{j,k}} (x_{i,k'} - x_{j,k'})^2 \\ &= \max\{x_{i,k}, x_{j,k}\}^2. \end{aligned}$$

Using this inequality, the inner product $\mathbf{C}_{k',:} \mathbf{q}$ is likewise bounded:

$$\begin{aligned} \mathbf{C}_{k',:} \mathbf{q} &= \sum_{i \in [n]} \left[\sum_{l \in \mathcal{D}_i} q_{il} (x_{i,k'} - x_{l,k'})^2 - \sum_{j \in \mathcal{S}_i} q_{ij} (x_{i,k'} - x_{j,k'})^2 \right] \\ &\leq \sum_{i \in [n]} \sum_{l \in \mathcal{D}_i} q_{il} \max\{x_{i,k}, x_{l,k}\}^2. \end{aligned}$$

Similarly, the norm $\|\mathbf{C}_{k',:}\|_2$ is bounded:

$$\begin{aligned} \|\mathbf{C}_{k',:}\|_2 &= \sqrt{\sum_{i \in [n]} \left[\sum_{l \in \mathcal{D}_i} (x_{i,k'} - x_{l,k'})^4 + \sum_{j \in \mathcal{S}_i} (x_{i,k'} - x_{j,k'})^4 \right]} \\ &\leq \sqrt{\sum_{i \in [n]} \left[\sum_{l \in \mathcal{D}_i} \max\{x_{i,k}, x_{l,k}\}^4 + \sum_{j \in \mathcal{S}_i} \max\{x_{i,k}, x_{j,k}\}^4 \right]}. \end{aligned}$$

Therefore, $\mathbf{C}_{k',:} \mathbf{q} + r \|\mathbf{C}_{k',:}\|_2$ is bounded by $\text{Prune}(k|\mathbf{q}, r)$.

C Proof of Lemma 4.2

First, we consider the first term of $\mathbf{C}_{k',:} \mathbf{q} + r \|\mathbf{C}_{k',:}\|_2$:

$$\mathbf{C}_{k',:} \mathbf{q} = \sum_{i \in [n]} \underbrace{\left[\sum_{l \in \mathcal{D}_i} q_{il} (x_{i,k'} - x_{l,k'})^2 - \sum_{j \in \mathcal{S}_i} q_{ij} (x_{i,k'} - x_{j,k'})^2 \right]}_{:=\text{diff}}.$$

Now, $x_{i,k'} \in \{0, 1\}$ is assumed. Then, if $x_{i,k'} = 0$, we obtain

$$\text{diff} = \sum_{l \in \mathcal{D}_i} q_{il} x_{l,k'} - \sum_{j \in \mathcal{S}_i} q_{ij} x_{j,k'} \leq \sum_{l \in \mathcal{D}_i} q_{il} x_{l,k}.$$

Meanwhile, if $x_{i,k'} = 1$, we have $x_{i,k} = 1$ from the monotonicity, and subsequently

$$\text{diff} = \sum_{l \in \mathcal{D}_i} q_{il} (1 - x_{l,k'}) - \sum_{j \in \mathcal{S}_i} q_{ij} (1 - x_{j,k'}) \leq \sum_{l \in \mathcal{D}_i} q_{il} - \sum_{j \in \mathcal{S}_i} q_{ij} (1 - x_{j,k}).$$

By using “max”, we can unify these two upper bounds into

$$\mathbf{C}_{k',:} \mathbf{q} \leq \sum_{i \in [n]} \max \left\{ \sum_{l \in \mathcal{D}_i} q_{il} x_{l,k}, x_{i,k} \left[\sum_{l \in \mathcal{D}_i} q_{il} - \sum_{j \in \mathcal{S}_i} q_{ij} (1 - x_{j,k}) \right] \right\}.$$

Employing a similar concept, the norm of $\mathbf{C}_{k',:}$ can also be bounded by

$$\begin{aligned} \|\mathbf{C}_{k',:}\|_2 &= \sqrt{\sum_{i \in [n]} \left[\sum_{l \in \mathcal{D}_i} (x_{i,k'} - x_{l,k'})^4 + \sum_{j \in \mathcal{S}_i} (x_{i,k'} - x_{j,k'})^4 \right]} \\ &\leq \sqrt{\sum_{i \in [n]} \left[\sum_{l \in \mathcal{D}_i} \max\{x_{i,k}, x_{l,k}\}^4 + \sum_{j \in \mathcal{S}_i} \max\{x_{i,k}, x_{j,k}\}^4 \right]}. \end{aligned}$$

Thus, we obtain

$$\text{Prune}(k) := \sum_{i \in [n]} \max \left\{ \sum_{l \in \mathcal{D}_i} q_{il} x_{l,k}, x_{i,k} \left[\sum_{l \in \mathcal{D}_i} q_{il} - \sum_{j \in \mathcal{S}_i} q_{ij} (1 - x_{j,k}) \right] \right\} + r \sqrt{\sum_{i \in [n]} \left[\sum_{l \in \mathcal{D}_i} \max\{x_{i,k}, x_{l,k}\} + \sum_{j \in \mathcal{S}_i} \max\{x_{i,k}, x_{j,k}\} \right]}.$$

D Proof of Theorem 4.1 (DGB)

From the 1/2-strong convexity of $-D_\lambda(\boldsymbol{\alpha})$, for any $\boldsymbol{\alpha} \geq \mathbf{0}$ and $\boldsymbol{\alpha}^* \geq \mathbf{0}$, we obtain

$$D_\lambda(\boldsymbol{\alpha}) \leq D_\lambda(\boldsymbol{\alpha}^*) + \nabla D_\lambda(\boldsymbol{\alpha}^*)^\top (\boldsymbol{\alpha} - \boldsymbol{\alpha}^*) - \frac{1}{4} \|\boldsymbol{\alpha} - \boldsymbol{\alpha}^*\|_2^2. \quad (37)$$

Applying weak duality $P_\lambda(\mathbf{m}) \geq D_\lambda(\boldsymbol{\alpha}^*)$ and the optimality condition of the dual problem $\nabla D_\lambda(\boldsymbol{\alpha}^*)^\top (\boldsymbol{\alpha} - \boldsymbol{\alpha}^*) \leq 0$ to (37), we obtain DGB.

E Proof of Theorem 4.2 (RPB)

From the optimality condition of the dual problem (5),

$$\nabla_{\boldsymbol{\alpha}} D_{\lambda_0}(\boldsymbol{\alpha}_0^*)^\top \left(\frac{\lambda_0}{\lambda_1} \boldsymbol{\alpha}_1^* - \boldsymbol{\alpha}_0^* \right) \leq 0, \quad (38)$$

$$\nabla_{\boldsymbol{\alpha}} D_{\lambda_1}(\boldsymbol{\alpha}_1^*)^\top \left(\frac{\lambda_1}{\lambda_0} \boldsymbol{\alpha}_0^* - \boldsymbol{\alpha}_1^* \right) \leq 0. \quad (39)$$

Here, the gradient vector for the optimal solution is

$$\begin{aligned} \nabla D_{\lambda_i}(\boldsymbol{\alpha}_i^*) &= -\frac{1}{2} \boldsymbol{\alpha}_i^* + \mathbf{t} - \mathbf{C}^\top \mathbf{m}_{\lambda_i}(\boldsymbol{\alpha}_i^*) \\ &= -\frac{1}{2} \boldsymbol{\alpha}_i^* + \mathbf{t} - \mathbf{C}^\top \mathbf{m}_i^*. \end{aligned}$$

Thus, by substituting this equation into (38) and (39), we get

$$\left(-\frac{1}{2} \boldsymbol{\alpha}_0^* + \mathbf{t} - \mathbf{C}^\top \mathbf{m}_0^* \right)^\top \left(\frac{\lambda_0}{\lambda_1} \boldsymbol{\alpha}_1^* - \boldsymbol{\alpha}_0^* \right) \leq 0, \quad (40)$$

$$\left(-\frac{1}{2} \boldsymbol{\alpha}_1^* + \mathbf{t} - \mathbf{C}^\top \mathbf{m}_1^* \right)^\top \left(\frac{\lambda_1}{\lambda_0} \boldsymbol{\alpha}_0^* - \boldsymbol{\alpha}_1^* \right) \leq 0. \quad (41)$$

From $\lambda_1 \times (40) + \lambda_0 \times (41)$,

$$\left(-\frac{1}{2} [\boldsymbol{\alpha}_0^* - \boldsymbol{\alpha}_1^*] - \mathbf{C}^\top [\mathbf{m}_0^* - \mathbf{m}_1^*] \right)^\top (\lambda_0 \boldsymbol{\alpha}_1^* - \lambda_1 \boldsymbol{\alpha}_0^*) \leq 0. \quad (42)$$

From (34),

$$\mathbf{C} \boldsymbol{\alpha}_i = \lambda_i \eta \mathbf{m}_i + \lambda_i \mathbf{1} - \boldsymbol{\beta}_i. \quad (43)$$

By substituting equation (43) into equation (42), we get

$$-\frac{1}{2} [\boldsymbol{\alpha}_0^* - \boldsymbol{\alpha}_1^*]^\top (\lambda_0 \boldsymbol{\alpha}_1^* - \lambda_1 \boldsymbol{\alpha}_0^*) - [\mathbf{m}_0^* - \mathbf{m}_1^*]^\top (\lambda_0 \lambda_1 \eta [\mathbf{m}_1 - \mathbf{m}_0] - \lambda_0 \boldsymbol{\beta}_1^* + \lambda_1 \boldsymbol{\beta}_0^*) \leq 0.$$

Transforming this inequality by completing the square with the complementary conditions $\mathbf{m}_i^{*\top} \boldsymbol{\beta}_i^* = 0$ and $\mathbf{m}_1^{*\top} \boldsymbol{\beta}_0^*, \mathbf{m}_0^{*\top} \boldsymbol{\beta}_1^* \geq 0$, we obtain

$$\left\| \boldsymbol{\alpha}_1^* - \frac{\lambda_0 + \lambda_1}{2\lambda_0} \boldsymbol{\alpha}_0^* \right\|_2^2 + 2\lambda_1 \eta \|\mathbf{m}_0^* - \mathbf{m}_1^*\|_2^2 \leq \left\| \frac{\lambda_0 - \lambda_1}{2\lambda_0} \boldsymbol{\alpha}_0^* \right\|_2^2.$$

Applying $\|\mathbf{m}_0^* - \mathbf{m}_1^*\|_2^2 \geq 0$ to this inequality, we obtain RPB.

Algorithm 4: General WS Method

1 initialize $\mathbf{x}_0 \in \mathcal{D}$
2 **for** $t = 1, 2, \dots$ **until** converged **do**
3 $\mathcal{W}_t = \{j \mid h_j(\mathbf{x}_{t-1}) \geq 0\}$
4 $\mathbf{x}_t = \arg \min_{\mathbf{x} \in \mathcal{D}} f(\mathbf{x})$ s.t. $h_j(\mathbf{x}) \leq 0, \forall j \in \mathcal{W}_t$

F Proof of Theorem 4.3 (RRPB)

Considering a hypersphere that expands the RPB radius by $\frac{\lambda_0 + \lambda_1}{2\lambda_0}\epsilon$ and replaces the RPB center with $\frac{\lambda_0 + \lambda_1}{2\lambda_0}\boldsymbol{\alpha}_0$, we obtain

$$\left\| \boldsymbol{\alpha}_1^* - \frac{\lambda_0 + \lambda_1}{2\lambda_0} \boldsymbol{\alpha}_0 \right\|_2 \leq \frac{|\lambda_0 - \lambda_1|}{2\lambda_0} \|\boldsymbol{\alpha}_0^*\|_2 + \frac{\lambda_0 + \lambda_1}{2\lambda_0} \epsilon.$$

Because ϵ is defined by $\|\boldsymbol{\alpha}_0^* - \boldsymbol{\alpha}_0\|_2 \leq \epsilon$, this sphere covers any RPB made by $\boldsymbol{\alpha}_0^*$ which satisfies $\|\boldsymbol{\alpha}_0^* - \boldsymbol{\alpha}_0\|_2 \leq \epsilon$. Using the reverse triangle inequality

$$\|\boldsymbol{\alpha}_0^*\|_2 - \|\boldsymbol{\alpha}_0\|_2 \leq \|\boldsymbol{\alpha}_0^* - \boldsymbol{\alpha}_0\|_2 \leq \epsilon,$$

the following is obtained.

$$\left\| \boldsymbol{\alpha}_1^* - \frac{\lambda_0 + \lambda_1}{2\lambda_0} \boldsymbol{\alpha}_0 \right\|_2 \leq \frac{|\lambda_0 - \lambda_1|}{2\lambda_0} (\|\boldsymbol{\alpha}_0\|_2 + \epsilon) + \frac{\lambda_0 + \lambda_1}{2\lambda_0} \epsilon.$$

By rearranging this, RRPB is obtained.

G Proof for Theorem 4.6 (RSS), 4.7 (RSP) and 4.8 (RSP for binary feature)

Here, we address only Theorems 4.6 and 4.7 because Theorem 4.8 can be derived in almost the same way as Theorem 4.7. When $\lambda_1 = \lambda$ is set in RRPB, the center and the radius of the bound $\mathcal{B} = \{\boldsymbol{\alpha} \mid \|\boldsymbol{\alpha} - \mathbf{q}\|_2^2 \leq r^2\}$ are $\mathbf{q} = \frac{\lambda_0 + \lambda}{2\lambda_0} \boldsymbol{\alpha}_0$ and $r = \left\| \frac{\lambda_0 - \lambda}{2\lambda_0} \boldsymbol{\alpha}_0 \right\|_2 + \left(\frac{\lambda_0 + \lambda}{2\lambda_0} + \frac{|\lambda_0 - \lambda|}{2\lambda_0} \right) \epsilon$, respectively. Substituting these \mathbf{q} and r into (16) and (17), respectively, and rearranging them, we can obtain the range in which the screening and pruning conditions hold.

H Proof of Theorem 4.9 (Convergence of WS)

By introducing a new variable \mathbf{s} , the dual problem (5) can be written as

$$\begin{aligned} \max_{\boldsymbol{\alpha} \geq \mathbf{0}, \mathbf{s} \geq \mathbf{0}} \quad & -\frac{1}{4} \|\boldsymbol{\alpha}\|^2 + \mathbf{t}^\top \boldsymbol{\alpha} - \frac{1}{2\lambda\eta} \|\mathbf{s}\|^2 \\ \text{s.t.} \quad & \mathbf{C}\boldsymbol{\alpha} - \lambda\mathbf{1} - \mathbf{s} \leq \mathbf{0}. \end{aligned}$$

We demonstrate the convergence of the WS method on a more general convex problem as follows:

$$\mathbf{x}^* := \arg \min_{\mathbf{x} \in \mathcal{D}} f(\mathbf{x}) \text{ s.t. } h_i(\mathbf{x}) \leq 0, \forall i \in [n], \quad (44)$$

where $f(\mathbf{x})$ is a γ -strong convex function ($\gamma > 0$). Here, as shown in Algorithm 4, the working set is defined by $\mathcal{W}_t = \{j \mid h_j(\mathbf{x}_{t-1}) \geq 0\}$ at every iteration. Then, the updated working set includes all the violated constraints and the constraints on the boundary. We show that Algorithm 4 finishes with finite T -steps and returns the optimal solution $\mathbf{x}_T = \mathbf{x}^*$.

Table 10: Total times for the path-wise optimization (sec).

Dataset Method \ Process	BZR			DD			FRANKENSTEIN		
	Traverse	Solve	Total	Traverse	Solve	Total	Traverse	Solve	Total
SSP	1397.1		4281.9	4292.9		13961.3	249.1		5013.0
	± 91.7	2884.8	± 964.1	± 388.3	9668.4	± 1580.6	± 9.3	4763.9	± 442.4
RSSP	539.2	± 934.5	3424.0	1132.2	± 1267.5	10800.6	189.7	± 441.5	4953.6
	± 47.2		± 956.9	± 118.0		± 1354.9	± 8.4		± 439.1
WSP	2448.5		2724.3	5888.3		7652.8	380.1		938.3
	± 170.8	275.8	± 184.9	± 465.6	1764.5	± 622.6	± 12.4	558.2	± 57.5
WSP+	565.5	± 68.5	841.3	946.1	± 195.6	2710.6	233.0	± 56.5	791.1
RSSP	± 49.7		± 97.3	± 83.1		± 258.6	± 11.7		± 55.7

Proof. Because f is γ -strong convex from the assumption, the following inequality holds:

$$f(\mathbf{x}_{t+1}) \geq f(\mathbf{x}_t) + \nabla f(\mathbf{x}_t)^\top (\mathbf{x}_{t+1} - \mathbf{x}_t) + \frac{\gamma}{2} \|\mathbf{x}_{t+1} - \mathbf{x}_t\|^2. \quad (45)$$

At step t , the problem can be written using only the active constraint at the optimal solution \mathbf{x}_t as follows:

$$\begin{aligned} \mathbf{x}_t &= \arg \min_{\mathbf{x} \in \mathcal{D}} f(\mathbf{x}) \text{ s.t. } h_i(\mathbf{x}) \leq 0, \forall i \in \mathcal{W}_t \\ &= \arg \min_{\mathbf{x} \in \mathcal{D}} f(\mathbf{x}) \text{ s.t. } h_i(\mathbf{x}) \leq 0, \forall i \in \{j \in \mathcal{W}_t \mid h_j(\mathbf{x}_t) = 0\} \end{aligned} \quad (46)$$

From the definition of \mathcal{W}_t , the working set \mathcal{W}_{t+1} must contain all active constraints $\{j \in \mathcal{W}_t \mid h_j(\mathbf{x}_t) = 0\}$ at the step t and can contain other constraints that are not included in \mathcal{W}_t . This means that \mathbf{x}_{t+1} must be in the feasible region of the optimization problem at the step t (46):

$$\mathcal{F} := \{\mathbf{x} \in \mathcal{D} \mid h_i(\mathbf{x}) \leq 0, \forall i \in \{j \in \mathcal{W}_t \mid h_j(\mathbf{x}_t) = 0\}\}$$

Therefore, from the optimality condition of the optimization problem (46),

$$\nabla f(\mathbf{x}_t)^\top (\mathbf{x}_{t+1} - \mathbf{x}_t) \geq 0, \mathbf{x}_{t+1} \in \mathcal{F}. \quad (47)$$

From the inequalities (45) and (47), we obtain

$$f(\mathbf{x}_{t+1}) \geq f(\mathbf{x}_t) + \frac{\gamma}{2} \|\mathbf{x}_{t+1} - \mathbf{x}_t\|^2.$$

If \mathbf{x}_t is not optimal, there exists at least one violated constraint $h_{j'}(\mathbf{x}_t) > 0$ for some j' because otherwise \mathbf{x}_t is optimal. Then, we see $\mathbf{x}_{t+1} \neq \mathbf{x}_t$ because \mathbf{x}_{t+1} should satisfy the constraint $h_{j'}(\mathbf{x}_{t+1}) \leq 0$. If $\mathbf{x}_t \neq \mathbf{x}_{t+1}$, from $\|\mathbf{x}_{t+1} - \mathbf{x}_t\|^2 > 0$,

$$f(\mathbf{x}_{t+1}) \geq f(\mathbf{x}_t) + \frac{\gamma}{2} \|\mathbf{x}_{t+1} - \mathbf{x}_t\|^2 > f(\mathbf{x}_t).$$

Thus, the objective function always strictly increases ($f(\mathbf{x}_t) < f(\mathbf{x}_{t+1})$). This indicates that the algorithm never encounters the same working set \mathcal{W}_t as the set of other iterations $t' \neq t$. For any step t , the optimal value $f(\mathbf{x}_t)$ with a subset of the original constraints \mathcal{W}_t must be smaller than or equal to the optimal value $f(\mathbf{x}^*)$ of original problem (44) with all constraints. Therefore, $f(\mathbf{x}_t) \leq f(\mathbf{x}^*)$ is satisfied, and we obtain $f(\mathbf{x}_T) = f(\mathbf{x}^*)$ at some finite step T . \square

I CPU Time for Other Datasets

Table 10 lists the computational times on the BZR, DD, and FRANKENSTEIN datasets. We first note that RSSP was approximately 2–4 times faster in terms of the traversal time compared with SSP. Next, comparing RSSP and WSP, we see that RSSP was faster for Traverse, and WSP was faster for Solve, as we observed in Table 2. Thus, the combination of WS&SP and RSSP was the fastest for all three datasets in total.

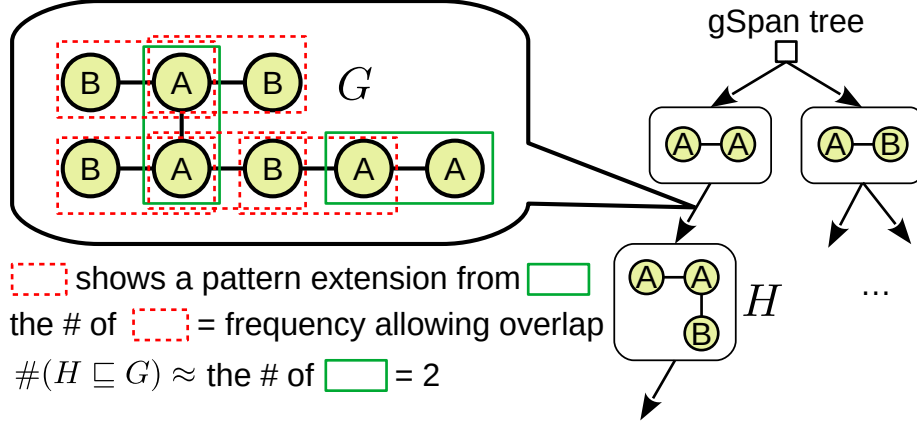


Figure 11: Approximation of $\#(H \subseteq G)$.

J Approximating Frequency Without Overlap

Let $F_G(H)$ be “frequency without overlap” that is the frequency of a subgraph of a given graph where any shared vertices and edges are disallowed for counting. This $F_G(H)$ is non-increasing with respect to the growth of H , but computing it is computationally complicated. Assuming that we know where all the subgraphs H appear in graph G , calculating $F_G(H)$ is equivalent to the problem of finding the maximum independent set, which is NP-complete (Schreiber and Schwöbbermeyer, 2005). In this section, using information obtained in the process of generating the gSpan tree, we approximate the frequency without overlap by its upper bound. This upper bound is also a lower bound of the frequency with overlap.

Figure 11 shows the process of generating the gSpan tree and frequency. In the figure, we consider the frequency of the subgraph H (\textcircled{A} - \textcircled{A} - \textcircled{B}) contained in the graph G . The graph H is obtained as a pattern extension of graph \textcircled{A} - \textcircled{A} (green frame) by \textcircled{A} - \textcircled{B} (red frame). gSpan stores the number of these pattern extensions at each traverse node. We define the count by this extension as $F_G^{\max}(H)$ (e.g., $F_G^{\max}(H) = 5$ for \textcircled{A} - \textcircled{A} - \textcircled{B}). Note that $F_G^{\max}(H)$ is the frequency of H allowing overlap and duplicately counting matches that are equivalent except for the index of nodes (e.g., $F_G^{\max}(H)$ for \textcircled{A} - \textcircled{A} - \textcircled{B} - \textcircled{A} - \textcircled{A} is two in the figure). Suppose that H currently has $e(> 1)$ edges (for example, $e = 2$ in \textcircled{A} - \textcircled{A} - \textcircled{B}). We recursively go back the traverse tree (a tree in the right of Figure 11) until we reach $e = 1$, i.e., the starting edge that generates H (in the case of \textcircled{A} - \textcircled{A} - \textcircled{B} , the starting edge is \textcircled{A} - \textcircled{A}). We use the number of unique matches of this starting edges (the number of green frames), which we define as $F_G^{\text{approx}}(H)$, as an approximation of $F_G(H)$. Obviously, $F_G^{\text{approx}}(H)$ is less than or equal to $F_G^{\max}(H)$. In the example, the number of green frames must be less than or equal to the number of red frames. Further, because only overlaps on the starting edge $e = 1$ are considered instead of overlaps in entire H , $F_G^{\text{approx}}(H)$ is greater than or equals to $F_G(H)$. Therefore, overall, we have $F_G(H) \leq F_G^{\text{approx}}(H) \leq F_G^{\max}(H)$. Unfortunately, from the definition, $F_G^{\text{approx}}(H)$ gives the same value whenever H has the same starting edge. However, this means that $F_G^{\text{approx}}(H)$ satisfies the monotonicity constraint for our pruning. Because the subgraph counting is a difficult problem and is not the main focus of our study, we employ $F_G^{\text{approx}}(H)$ as a simple approximation. For our framework, any approximation is applicable given that it satisfies the monotonicity constraint.